New Semi-Solid Electrolytes for Mass Production and Increased Lifetime of Dye Solar Cells

Aapo Poskela

School of Science

Thesis submitted for examination for the degree of Master of Science in Technology.
Espoo 24.1.2017.

Thesis supervisor:

Prof. Peter Lund

Thesis advisor:

D.Sc. (Tech.) Kati Miettunen

Aalto University
School of Science

AALTO UNIVERSITY
SCHOOL OF SCIENCE

ABSTRACT OF THE
MASTER'S THESIS

Author: Aapo Poskela

Title: New Semi-Solid Electrolytes for Mass Production and Increased Lifetime of Dye Solar Cells

Date: 24.1.2017 Language: English Number of pages: 7+52

Department of Applied Physics

Professorship: Energy Sciences SCI3056

Supervisor: Prof. Peter Lund

Advisor: D.Sc. (Tech.) Kati Miettunen

This study focuses on improving either mass production or lifetime of dye solar cells. The first goal was to study how the state of the external circuit affects the degradation of dye solar cells under illumination. This effect is relevant when considering the operation and aging of cells in actual use. Cells were aged in open circuit, short circuit and under a load close to their maximum power point. It was determined that aging in short circuit had clearly detrimental effect on the long-term stability of the cells, while cells in open circuit and under load performed similarly to each other. The reasons for the different behaviours of the cells was discussed further based on the extensive measurements performed on the cells before, during and after the aging. The cause of the rapid decrease in the performance of short circuited cells was identified to be the degradation of charge carriers in the electrolyte.

The second goal was to discover a method to increase dye solar cell stability by adding absorber polymers into the electrolyte of the cells. The hypothesis was that the absorbing polymers would absorb water, which is generally harmful to dye solar cells, during the operation of the cells thus allowing the cells to function longer. Unfortunately, the polymers decreased cell performance notably. As the degradation was apparent instantly after the cell assembly, it is likely that the polymers reacted with the electrolyte of the cells.

The final goal was to enhance dye solar cell fabrication methods with the help of biomaterial aerogels. The usual method of injecting liquid electrolyte into a cell through small holes in the substrates has few practical issues, especially when filling a cell with a large area. In this work the aerogels were inserted between the electrodes of the cells and then soaked in electrolyte before the cell was sealed. The aerogels successfully held the liquid electrolyte in place, thus also improving the cell resistance against leaking. The measurements also indicated that this assembly method avoided the problems present in injecting the electrolyte. The performance of the cells assembled with the best of the aerogels did not differ from the performance of the reference cells, demonstrating the validity of this assembly technique.

Keywords: Dye solar cell, stability, mass production, semi-solid, electrolyte, aging, absorbers, biomaterials

AALTO-YLIOPISTO
PERUSTIETEIDEN KORKEAKOULU

DIPLOMITYÖN
TIIVISTELMÄ

Tekijä: Aapo Poskela

Työn nimi: Uusia puolikiinteitä elektrolyyttimateriaaleja väriaineaurinkokennojen stabiiliuden parantamiseksi ja massatuotannon helpottamiseksi

Päivämäärä: 24.1.2017 Kieli: Englanti Sivumäärä: 7+52

Teknillisen fysiikan laitos

Professuuri: Energiatieteet SCI3056

Valvoja: Prof. Peter Lund

Ohjaaja: Dos. Kati Miettunen

Tämän työn päätavoitteet kohdistuvat väriaineaurinkokennojen massatuotannon ja niiden eliniän parantamiseen. Ensimmäinen tavoite oli selvittää miten väriaineaurinkokennoon kytketty virtapiiri vaikuttaa valaistun kennon degradaatioon. Virtapiirin vaikutus on tärkeää huomioida tutkittaessa aurinkokennojen ikääntymistä oikeassa käytössä. Kennoja ikäännytettiin avoimessa ja oikosuljetussa piirissä, sekä kytkettynä kuormaan joka vastasi kennon maksimitehopistettä. Selvisi että oikosulku vaikutti selvästi haitallisesti kennojen stabiiliuteen, kun taas kennot kuormassa ja avoimessa piirissä ikääntyivät keskenään hyvin samankaltaisesti. Erilaisten ikääntymisprosessien syitä analysoidaan työssä lisää kattavien, koko ikäännytyksen ajan tehtyjen, mittausten pohjalta. Oikosuljettujen kennojen nopean ikääntymisen syyksi tunnistettiin elektrolyytin varauksenkuljettajien nopea degradaatio.

Toinen tavoite oli parantaa väriaineaurinkokennojen käyttöikää lisäämällä elektrolyyttiin polymeerejä, jotka kykenevät absorboimaan vettä. Suunnitelmana oli, että polymeerit absorboisivat yleensä kennoille haitallista vettä kennon toiminnan aikana, siten mahdollistaen kennoille pidemmän toiminta-ajan. Valitettavasti polymeerit heikensivät kennojen suorituskykyä huomattavasti. Koska kennot heikkenivät heti polymeerin lisäämisen jälkeen, on todennäköistä että polymeerit reagoivat jonkin elektrolyytin ainesosan kanssa välittömästi.

Viimeisenä tavoitteena oli väriaineaurinkokennojen valmistusmenetelmien tehostaminen biomateriaali-aerogeelien avulla. Tavallisesti kennoihin lisätään nestemäinen elektrolyytti injektoimalla se substraatissa olevista aukoista, millä on kuitenkin muutamia haittapuolia, varsinkin täytettäessä suurta kennoa. Tässä työssä aerogeelit asetettiin kennon elektrodien väliin ja kasteltiin elektrolyytillä ennen kennojen sulkemista. Aerogeelit myös onnistuivat pitämään nestemäisen elektrolyytin paikoillaan, mikä myös lisää kennojen mekaanista kestävyyttä vuotoja vastaan. Mittaukset myös indikoivat, että tämä valmistusmenetelmä vältti injektiossa esiintyvät ongelmat. Parhaan aerogeelin avulla kasattujen kennojen suorituskyky ei eronnut referenssikennojen suorituskyvystä, mikä demonstroi tämän menetelmän toimivuutta.

Avainsanat: väriaineaurinkokenno, stabiilius, massatuotanto, puolikiinteä, elektrolyytti, ikäännytys, absorbointi, biomateriaalit

Preface

I would like to give my heartfelt thanks to my instructor D.Sc. Kati Miettunen. This Master's thesis, or any of my previous works, would not even exist without your guidance. My supervisor, Prof. Peter Lund, also deserves my thanks for giving me the possibility to work at his New Energy Technologies-research group here at Aalto University. Writing down everything I have learned while working here would fill a dozen Master's theses. Big thanks also belong to a fellow Master's thesis worker: Mr. Sakari Lepikko, for constant teamwork ranging from assembling a shared cell series to discussions on numerous topics. I am also grateful to M.Sc. Armi Tiihonen for the varied and insightful discussions, for the help on the use of the weather chamber and for the several MatLab scripts that hastened the analysis of the measurement results of this work. I thank also the rest of my co-workers for companionship and for the, more and less serious, coffee table discussions over the years.

I owe gratitude for my landlady D.Sc. Jaana Vapaavuori from Tampere University of Technology and University of Montreal for the idea and materials used for the absorber polymer experiments.

I am also grateful for the help of researchers from the Department of Forest Products Engineering: the biomaterial aerogels were prepared by D.Sc. Maryam Borghei and M.Sc. Janika Lehtonen from the group of Prof. Orlando Rojas. I also enjoyed the teamwork involved in preparing the lab course with D.Sc. Maryam Borghei.

Thanks also belong to the Academy of Finland (SOLID) for the funding of this study.

Last but not least, I would like to thank my family and friends for all of their unwavering support during this work. My family supported me in any way they could, even making sure I was kept fed during the busiest times. My friends allowed me to relax, forcing my mind away from the work by taking me along on all kinds of adventures.

Aapo Poskela
Otaniemi, 24.1.2017

Contents

Symbols and abbreviations

Symbols

$c_{I_3^-}$	Concentration of I_3^-
C_{CE}	Electrolyte-counter electrode interface capacitance
C_{CO}	TiO_2-conducting substrate interface capacitance
C_μ	Recombination capacitance
C_{SU}	Electrolyte-conducting substrate capacitance
$D_{I_3^-}$	Diffusion coefficient of I_3^-
d	Diffusion distance
E_g	Bandgap energy
F	Faraday constant
FF	Fill factor
I_{lim}	Limiting current
I_{SC}	Short circuit current
k_B	Boltzmann constant
λ	Wavelength
ω	Angular frequency
P_{max}	Maximum power point
q_e	Elementary charge
Φ	Incident photon flux
R_{CO}	TiO_2-conducting substrate interface resistance
R_{CE}	Electrolyte-counter electrode charge transfer resistance
R_D	Diffusion resistance of the electrolyte
R_S	Ohmic series resistance of the cell
r_T	Transport resistances in the TiO_2 film
R_{PE}	Combined photoelectrode resistance
r_{REC}	Charge recombination resistance
R_{SU}	Electrolyte-conducting substrate interface resistance
T	Temperature
V_{OC}	Open circuit voltage
η	Efficiency
η_{IPCE}	Incident photon-to-charge carrier efficiency
η_{LH}	Light harvesting efficiency
η_{INJ}	Electron injection efficiency
η_{COL}	Electron collection efficiency
Z	Impedance
Z_D	Mass transport impedance of the electrolyte

Abbreviations

1Sun	Illumination intensity equivalent to 1000 W/m²
ACN	Acetonitrile
AM1.5G	Standardized condition where solar cell measurements are performed
BC	Bacterial Cellulose
DSC	Dye Solar Cell

EIS	Electrochemical Impedance Spectroscopy
FTO	Fluorine-doped Tin Oxide
GuSCN	Guanidinium thiocyanate
HOMO	Highest Occupied Molecular Level
I^-	Iodide
I_3^-	Tri-iodide
I_2	Iodine
IPCE	Incident Photon-to-Charge carrier Efficiency
IV	Current-Voltage
LUMO	Lowest Unoccupied Molecular Level
MPN	3-methoxypropionitrile
MPP	Maximum Power Point
NFC	Nano-Fibrillated Cellulose
NMBI	1-methyl-benzimidazole
PAA	Polyacrylic acid
PMII	1-propyl-3-methylimidazolium iodide
PMMA	Poly(methyl methacrylate)
PV	Photovoltaics
PVP	Polyvinylpyrrolidone
RGB	Red-Green-Blue
TBA	*tert*-buthanol
TBP	*tert*-butylpyridine
TCO	Transparent Conducting Oxide
TEMPO	TEMPO-mediated Oxidized Nano-Fibrillated Cellulose
$TiCl_4$	Titanium tetra-chloride
TiO_2	Titanium dioxide
Z907	cis-Bis(isothiocyanato)(2,2'-bipyridyl-4,4'-dicarboxylato)(4,4'-di-nonyl-2'-bipyridyl)ruthenium(II)

1. Introduction

For decades, burning fossil fuels has been responsible for producing energy to the needs of human society. In recent years, as the environmental impact and future sufficiency of fossil fuels is questioned, clean and renewable energy technologies are gaining more attention [1]. The increased attention has led to the development of several new energy technologies and branching of some older and established ones. Photovoltaic (PV) technologies have long been dominated by silicon solar cells, which rely on the properties of pn-junctions (interface between two differently doped semiconductors) to generate electricity. The field of PV technologies has however diversified in recent years with the emergence of several third generation solar cells, which are based on different power generation mechanisms [2]. While only few of these third generation cells can compete with silicon solar cells in terms of power conversion efficiency, these technologies promise low fabrication costs and simple manufacturing processes. Third generation solar cells can also be used in applications that cannot be fulfilled by silicon solar cell, such as demonstrating varied coloration, so there is no need for the different technologies to compete on the exactly same markets [3].

This work focuses on one of these third generation PV cells, dye solar cells (DSC). Dye solar cells (also called dye-sensitized solar cells or Grätzel cells) were first demonstrated in 1991 by Michael Grätzel and Brian O'Regan [4]. Ever since the DSCs have been steadily developed, and nowadays the best devices have achieved power conversion efficiency of 13% [5]. The most attractive features of DSCs are their low cost components, easy and flexible manufacturing methods and the possibility to fabricate differently colored cells by simply using different sensitizer dyes. These properties make DSCs a good option for use as a supporting energy source in small-scale electronic devices or as building integrated PV elements [6]. Unfortunately, DSCs have not yet been able to enter large-scale commercial production due to the relatively limited stability of most device configurations. The performance DSCs have been shown to degrade when the cell is exposed to light, high temperature or humidity and moisture [7]. Commonly DSCs also utilize a liquid-phase electrolyte, which brings further challenges to the assembly and stability of the cells; the cell will cease to function if the electrolyte manages to leak from the cell due to damaged or poor sealing. Another practical issue in the large-scale production of DSCs is related to their manufacturing methods and the liquid electrolyte: it has been shown that if the electrolyte is injected into the assembled cell, the nanoporous photoelectrode acts as a filter, which prevents an even distribution of the electrolyte components. This results in significant losses in the overall efficiency of the device [8].

In this work, several methods to address the issues introduced above are studied. The work is divided into three distinct experimental parts, each of which is focused on different aspect of DSC stability.

In the first part, the stability studies of DSCs themselves are discussed. The stability or 'aging' studies of DSCs lack any general guidelines, which results in great variation between different studies in literature. For example, the definition of a 'stable' solar cell varies greatly from an article to article and a DSC declared stable by one article, would not be such by the standards of another article. In addition, the stability tests the cells are subjected to vary greatly: while the aging

for 1000h under illumination has become somewhat standard, there is no agreement on the spectrum of the light used in the aging. Should it for example include UV light or not [9]? In addition, the cell temperature at the illumination aging and separate thermal tests varies. Some publications require stability in 60 °C, while according to others the DSCs should endure 80 °C or more for extended periods of time [10] [11]. DSC stability research would benefit greatly from the formation of a common set of guidelines, similar to those that have been created for the organic PV [12]. In this work, something that is rarely even considered in DSC aging studies is investigated: the state of the circuit where the DSCs are aged in. Most commonly DSCs are simply left in open circuit during the aging. Here a comparison is made between aging DSCs in open circuit, short circuit and under a load. The results suggest that cells aged in open circuit and under load perform similarly and are relatively stable. The short circuited cells however seem to degrade significantly faster than the others do. These results will be discussed in terms of what is relevant for future studies: for the ones done in this work and more broadly. In addition, the results from other studies in the literature are discussed and compared to what is discovered in this study.

The second part is focused on improving the long-term stability of DSCs. It has been shown that the performance of DSCs quickly degrades with water or other impurity intrusion into the cell [7]. We attempted to slow down this effect by adding commonly used absorber polymers into the cell, with the hypothesis that these would absorb any harmful impurities and thus allow the cells to function longer. Unfortunately, all of the absorbers appeared to cause harmful reactions in the cells, decreasing their performance instead of increasing their lifetime.

The goal of the third part was to present a method to improve the fabrication process of DSCs, similar to an earlier study [13]. This was realised by assembling the cells with a thin film of biomaterial aerogel in the electrolyte. The benefit of this method is that it allows the insertion of the liquid electrolyte into the cell simply by pipetting it on the aerogel, which then functions as a sponge, holding the electrolyte in place. This method avoids the adverse effects of electrolyte filtering that are present when the electrolyte is injected into the cell, as mentioned above. As an added benefit, DSC assembled with such an electrolyte sponge should be more mechanically robust, since the aerogel should hold the electrolyte in place even when the sealing of the cell is damaged. In addition to the easier manufacturing, the biomaterials could also work as impurity absorbers, which has not been investigated before. The best of the biomaterial aerogels tested here was bacterial cellulose. It successfully avoided the problems present with injected electrolyte and did not alter the performance of the cells compared to the reference cells. Chitin and nano-fibrillated cellulose successfully functioned as electrolyte sponge, but somewhat decreased the cell performance.

These studies were conducted by assembling multiple DSC devices in each of the different groups under study in order to improve the statistical significance of the results. Then the devices were aged under either lighting similar to the standard AM1.5G-spectrum, with the UV component of the light filtered away, or with strong UV lamps, depending on the goal of the study in question. The performance and its degradation was studied by multiple measurements: the current-voltage characteristics, electrochemical impedance and bleaching of the electrolyte was measured on constant intervals during the aging. Further information on the cells was gathered with additional measurements before and after the aging. These measurements included the quantum efficiency of the cell,

transmittance through the electrolyte of the cell and the dependence of the short circuit current of the cells on the illumination intensity.

2. Theory and background

This section describes the theoretical background of the topics discussed in this work. It aims to clarify the operation of the different dye solar cell types studied in this work and the requirements of an aging study for these cells.

2.1. Dye solar cells

Dye solar cells (DSC) are electrochemical devices that generate electricity through the photovoltaic effect. Their structure is illustrated in Figure 1 and the energy band configuration of this structure is given in Figure 2.

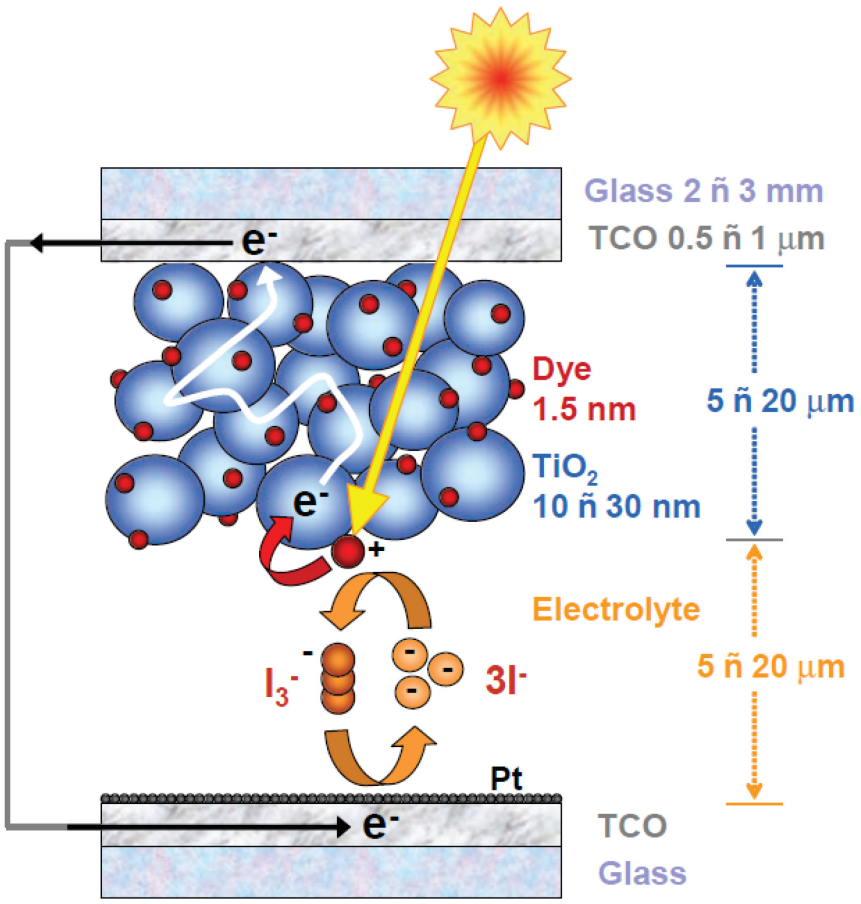

Figure 1 the schematic structure of DSC. [14]

In a DSC, a nanoporous semiconductor (usually TiO_2) is used to transport electrons and holes as charge carriers. Unlike in a silicon solar cell, the bandgap energy E_g of the TiO_2 is too high for a direct photoexcitation by incident visible light. This is mended by adsorbing Ruthenium complex photosensitizer dye on the surface of the semiconductor nanoparticles. The bandgap between the highest occupied molecular level (HOMO) and lowest unoccupied molecular level (LUMO) of these dyes is small enough to allow photoexcitation. Once electrons are excited from the HOMO level to the LUMO level of the dye, the goal is to inject these excited electrons to the conduction band of the TiO_2. The dye must be

selected so that its LUMO level has sufficiently higher energy than that of the conduction band of the TiO_2, which allows the excited electrons to swiftly inject into the TiO_2 [15] (see Figure 2). The porosity of the TiO_2 allows the dye to attach to a large surface area, thus increasing the efficiency of the light absorption. The electrons are transported through the TiO_2 layer, finally reaching the electric contact, which is connected to external circuit. The contact is usually a transparent conducting oxide (TCO) coated glass. The DSC is filled with electrolyte, which purpose is to regenerate the electrons to the dye after the dye has been oxidized by the injection of the electrons to the TiO_2. The electrolyte includes some redox mediator pair responsible for the redox reactions, usually tri-iodide (I_3^-) and iodide (I^-). The mediators oxidize when regenerating the dye, and then diffuse to the counter electrode where they are reduced by electrons from the external circuit. The counter electrode is covered with a catalyst layer to enhance the rate of this process. Thus, the redox reactions in the case of iodine are [15]:

$$I_3^- + 2e^- \leftrightarrow 3I^-. \tag{1}$$

The redox potential of the electrolyte must be adequately above the HOMO level of the dye to enable reaction that is fast enough. Overall, in ideal operation, there are no permanent chemical changes within the DSC.

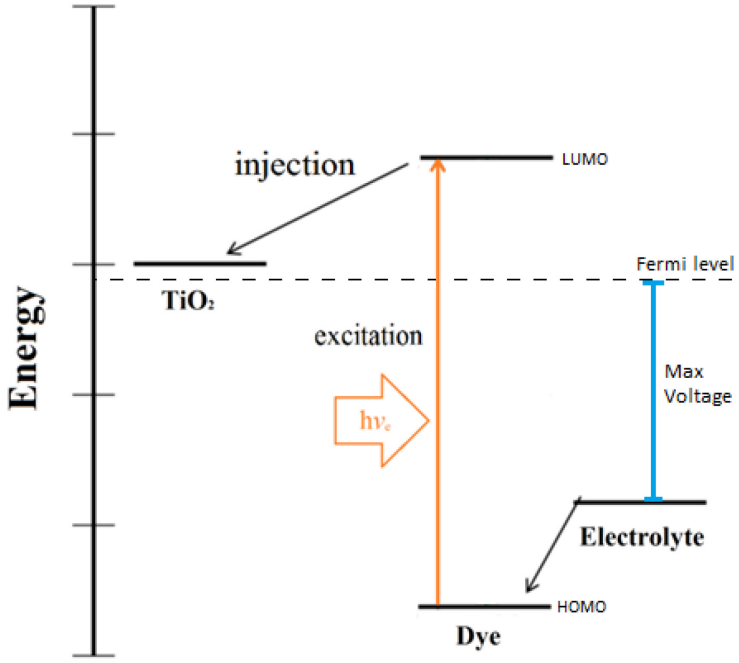

Figure 2 the energy level diagram of a typical DSC.

The performance of the DSC is adjusted by the relative positions of the energy levels of different components within the cell and by the bandgap of the dye. As illustrated in Figure 2, the expected voltage of the cell is the difference between the redox potential of the electrolyte and the Fermi level of the cell [15]. The redox potential must have higher energy than the dye HOMO level, which limits the choice of the electrolyte. In turn, the magnitude of the bandgap in the dye determines the amount of photocurrent that can be extracted from the cell.

Smaller bandgaps allow also longer wavelengths of light to be utilized. This has to be again balanced with the required relative positions of the dye LUMO level with the TiO_2 conduction band and the dye HOMO level with the redox potential level.

The above description of DSC operation is the ideal picture. In practice, several different loss mechanisms decrease the performance of the cell. After photoexcitation of the electrons in the dye, not all of those electrons are injected to the TiO_2, but some are relaxed back to the ground state in the dye. This relaxation rate competes with the injection rate, which can be increased by increasing the difference between the LUMO level of the dye and the conduction band of the TiO_2.

The injected electrons may also recombine with the ions in the electrolyte, a phenomenon that is called the dark current. The dark current can be greatly suppressed with some additives in the electrolyte. One such additive is *tert*-butylpyridine (TBP) which adsorbs to the surface of TiO_2, at locations without dye molecules, thus blocking dark current.

Finally, the power extracted from a cell is decreased by different resistances to charge transport. These include the usual ohmic resistances at the different contacts, the charge transfer resistances in different components and the diffusion resistance of the electrolyte.

2.2. Degradation of dye solar cells

Even though the operation of a solar cell is theoretically a fully reversible process, in reality the cells degrade over time. This process is often called aging. In DSCs many internal and external factors affect the rate of degradation, including all of the used materials and their concentrations within the cell, quality of the sealing of the cell, outside humidity, temperature, illumination intensity and spectrum, and the state of the cell (open-circuit, load, or short-circuit) [16]. Here, degradation mechanisms divided by the different cell components they affect are discussed.

The simplest case of degradation is a mechanical breaking of the cell. This can be caused by the application of strong mechanical stress (i.e. hitting or dropping the cell) or by the degradation of the sealing materials of the cell. Depending on the used sealing method, the cell can be degraded by temperature or by humidity and moisture. For example, a cell manufactured completely of glass is very well protected against high temperatures and high amounts moisture but may be shattered by relatively small applied forces. In contrast, a cell made on plastic substrates is mechanically very robust but water may permeate through it slowly [17]. Failure of the sealing of the cell can lead to evaporation or leakage of the electrolyte away from the cell or to intrusion of detrimental substances such as water into the cell. It is important to select a suitable sealing method for the desired application. Another method to decrease the risk of losing electrolyte is to use electrolytes that will not evaporate or leak, such as quasi-solid or solid electrolytes or ionic liquids [7].

Another external component that is sensitive to mechanical stresses and moisture are the current collectors of the cell. In addition to being accidentally cut, they may be corroded by long-term exposure to moisture. Iodine in the electrolyte also quickly corrodes most of the metals used in current collectors, so it is vital that they are kept separate [7].

Even if the cell is sealed well and protected from mechanical damage, the components within the cell can degrade through various detrimental reactions. The counter electrode for instance, may suffer during normal operation of a DSC. While the conducting substrate on the counter electrode is very stable, the successful operation of the cell depends on the catalytic layer over the counter electrode [7]. One of the degradation mechanisms of the catalyst is the detachment of catalyst particles from the TCO surface. The robustness of the contact is shown to be dependent on the deposition method of the catalyst [18]. The catalyst may also be degraded by corrosive reactions with the electrolyte or deposition of electrolyte by-products that block charge transfer [7].

The photoelectrode is also a possible target for many degradation mechanisms. Usually the degradation of the photoelectrode is attributed to reactions that affect the photosensitizer dye. High temperatures have been shown to cause dye desorption from the TiO_2 surface and dissolution into the electrolyte [7] [19]. Other hypotheses of dye degradation mechanisms include replacement of the dye molecules by decomposition products from the electrolyte and reactions between oxidized dye molecules and radicals in the electrolyte [7]. The degradation of the photoelectrode is not necessarily only related to the dye, but can also affect the TiO_2 layer. The degradation of the TiO_2 can often be detected as a decrease of electron lifetime within the film. This is a symptom of lowered recombination resistance, which can be caused contaminants adsorbing onto the TiO_2 surface and acting as recombination centers. Examples of such contaminants are detached and diffused catalyst particles from the counter electrode [7] and accumulated side products from the electrolyte, including small cations such as H^+ and Li^+ [20].

The degradation of a DSC is often caused by decreased performance of the electrolyte. Usually the electrolyte degradation is contributed to the loss of tri-iodide I_3^- from the electrolyte. Hypotheses have been formed which suggest that tri-iodide is either consumed in sublimation of iodine, in an irreversible reaction with an impurity like water [7] or the formation of iodate during the redox reaction of the electrolyte [21]. Another possible reaction that decreases the amount of tri-iodide in the electrolyte is a ligand exchange reaction between SCN^- of the dye and the tri-iodide [22]. The decrease of the tri-iodide limits charge transfer through the electrolyte, which results in a higher charge transfer resistance and a lower performance of the DSC. Decrease in tri-iodide concentration can be verified optically as it gives the iodine electrolyte its yellow color. When the concentration is decreased, the electrolyte is bleached and becomes almost transparent. The decrease of tri-iodide has been seen to be caused by high temperatures, introduction of water into the cell and UV light.

UV light and water are often considered the most obvious threats to DSC stability. UV light quickly degrades the cell performance through different mechanisms such as direct band excitations in TiO_2, which in turn can cause oxidation of the dye or electrolyte components [7]. The degradation due to UV can often be detected as bleaching of the electrolyte. To ensure that DSC can be used under UV illumination, they need to be protected for example with a UV filter [23]. Water has been shown to significantly reduce the performance of a DSC [7] [24], although the extent of the effect varies in different studies [25]. Introduction of water into the cell alters the conduction band position of the TiO_2, which leads to higher voltages, but is also expected to oxidize iodine [7] and increase recombination of the free charges [24], which causes lower performance and shorter lifetime for the cell. It is also possible that the UV and water

degradation are linked: UV light could cause water splitting in the solar cells and for instance hydroxide could be highly reactant towards the other cell components, in particular the electrolyte and the dye. To improve DSC stability, it seems necessary to avoid intrusion of water into the cell as much as possible, which should be taken into consideration during the cell assembly and sealing. Here, the use of different water absorbents is investigated. The hypothesis is that especially the presence of freely moving water should be avoided, for instance the UV light does not penetrate deep in to the cell and avoiding having water in the photoelectrode area should be critical in preventing reactions of water with UV light and the related adverse effects.

2.3. Measurement Techniques

Thorough characterization of DSCs requires multiple different measurement methods and equipment, several of which were used in this study. In this chapter, the theory behind each of the used methods is described shortly.

2.3.1. Current-Voltage characteristics

The most common and informative data acquisition method of the properties of a DSC, or of any type of solar cell, is the measuring of the IV curve of a cell. The standardized curve is obtained by setting the cell into steady state under 1000 W/m² illumination with lighting that has a good match with the standard AM1.5G-spectrum. Then the current through the cell is measured while sweeping the voltage applied to the cell. The sweep is usually a 2-way sweep in order to detect any hysteresis that may be caused by too fast sweep rate or by a cell that has not yet reached a steady state [15]. Since the current obtained from a solar cell depends on the size of the active area, current density is used instead to report the measured current, which makes comparison of different cells easier. A typical IV curve measured from a DSC is shown in Figure 3.

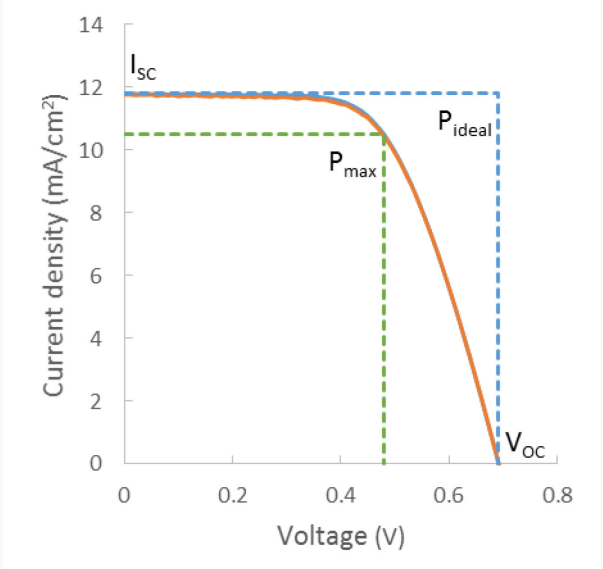

Figure 3 Example of a typical 2-way IV curve of a DSC. The locations of short circuit current I_{SC}, open circuit voltage V_{OC} and maximum power point P_{max} are shown. Fill factor FF is calculated as the ratio of the areas below P_{max} and P_{ideal}.

Several important cell parameters can be determined from the IV curve. The open circuit voltage V_{OC} and short circuit current I_{SC} can be directly determined from the points where the curve crosses the axes, i.e. when current or voltage are zero respectively. The maximum power point P_{max} is the point where the power $P=IV$ produced by the cell reaches its maximum. These values can be used to calculate the fill factor FF of solar cells that illustrates how ideally the cell operates.

$$FF = \frac{P_{max}}{P_{ideal}} = \frac{V_m I_m}{V_{OC} I_{SC}}. \quad (2)$$

The real P_{max} is always lower than the ideal P_{ideal} since the cell will suffer from some loss mechanisms, which are discussed in more detail in chapter 2.1. The solar energy conversion efficiency can then be calculated as a ratio of power output of the cell and the power of the incident radiation [26].

$$\eta = \frac{P_{out}}{P_{in}} = \frac{V_m I_m}{P_{in}} = \frac{FF \cdot V_{OC} I_{SC}}{P_{in}}. \quad (3)$$

Where P_{in} is the power of the incident light.

As mentioned earlier in this chapter, charge transfer in the electrolyte is performed by the diffusion of I_3^-/ I^- -redox mediator pair. It is possible, given high enough illumination intensity, too small amount of redox mediators or too obstructed path through the electrolyte, the current extracted from the cell becomes limited by the diffusion of the mediator pair. This is called the limiting current I_{lim}. The limiting current can be expressed mathematically by deriving from Fick's law [14] as:

$$I_{lim} = \frac{4F D_{I_3^-} c_{I_3^-}}{d}. \quad (4)$$

Where d is the diffusion distance, in this case the distance between the electrodes, F is the Faraday's constant, $D_{I_3^-}$ and $c_{I_3^-}$ are respectively the diffusion coefficient and concentration of I_3^-. The reason we use the diffusion constant and concentration of I_3^- is that in a typical DSC the equilibrium concentration of I_3^- is nine times lower than the concentration of I^- [14] and thus the charge transport is limited by I_3^-. Adding additional I_3^--ions will not improve the cell since excess amount of them increases recombination losses at the photoelectrode and decreases absorbtion of light by the dye by darkening the color of the electrolyte.

As a DSC is aged, some of the redox mediators degrade and are no longer useable in the charge transport or they have degraded so that they have a much more limited capacity to carry charge (see discussion in chapter 2.2). Thus, the concentration $c_{I_3^-}$ decreases and therefore, according to equation *(4)*, the limiting current I_{lim} decreases as well. Therefore, changes in the redox mediator concentration can be studied by varying the intensity of illumination on a solar cell and measuring the I_{SC} on different intensities. By performing such measurements on fresh and aged cells, the loss of charge carriers should become apparent as lower I_{SC} at high illumination intensities in the aged cells.

2.3.2. Electrochemical Impedance Spectroscopy

Electrochemical Impedance Spectroscopy (EIS) is a measurement method that is used to obtain more detailed information on the internal workings of an electrochemical device, in this case a DSC. EIS allows the characterization of different charge transfer parameters within a DSC, including for example interfacial resistances and capacitances [27]. The resistances correspond to different processes that impede charge transfer through the cell and the capacitances describe accumulation of charges at interfaces. The power of EIS measurements lies in the fact that different resistance/capacitance couples have different time constants so that they appear on different frequencies and can thus be separated in the EIS spectrum. To measure EIS from a DSC, the cell is set into a steady state operating condition i.e. the incident illumination, temperature and voltage of the cell are set to certain values, which are decided depending on which parameters we are interested in. Not all of the obtainable parameters can be measured at one voltage since the total cell resistance is not constant but depends nonlinearly on the operating point, as can be witnessed from the shape of the IV curve (Figure 3). Different assumptions on the model can be applied at different measurement conditions, which allows solving certain resistance and capacitance values. Once the cell is in a steady state, the voltage is varied with harmonic AC voltage modulation $V_{AC}(\omega,t)$, where the angular frequency ω is swept over a wide range of values. This will generate an AC current response, which is then measured and used to calculate the impedance [14]:

$$Z(\omega) = \frac{V_{AC}(\omega,t)}{i_{AC}(\omega,t)}. \tag{5}$$

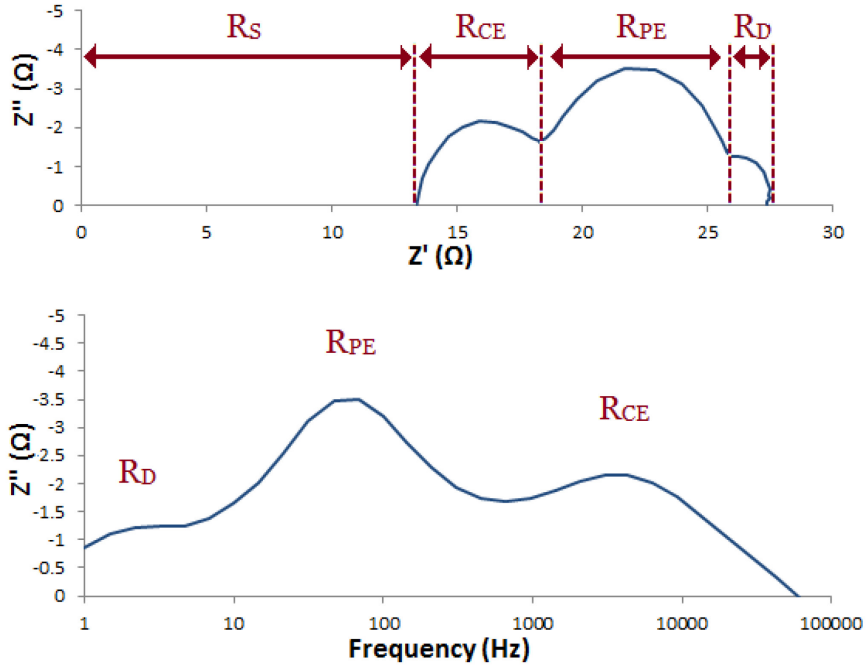

Figure 4 A Nyquist plot of an example DSC is shown in the upper figure. The different resistance components can be seen from the figure as shown above. The values obtained by performing a fit are R_S=13.1Ω, R_{CE}=5.2Ω, R_{PE}=7.0Ω and R_D=2.1Ω. The lower figure displays the dependence of the imaginary component of the impedance on the modulation frequency, which helps in recognizing which internal resistances are visible in the Nyquist plot.

To obtain the desired parameters, the impedance is plotted as a Nyquist curve, where the x-axis and y-axis are the real and imaginary component of the impedance, respectively. It is also useful to plot the imaginary impedance as a function of frequency (Bode plot), as this allows visual confirmation to which resistance elements are visible in the Nyquist plot if their characteristic frequencies are known. Examples of these curves are visible in Figure 4. The different resistances are visible as illustrated in the Figure 4: the start point of the Nyquist curve marks the amount of ohmic series resistance (R_S) in the cell and the three following semi-circles are from left to right: the charge transfer resistance at electrolyte-counter electrode interface (R_{CE}), the combined resistances of the photoelectrode (R_{PE}) and the diffusion resistance through the electrolyte (R_D). These are related to the equivalent circuit model of a DSC, which is discussed below. The internal impedances of the different components in a typical DSC have different time constants which enables distinguishing them from each other with AC voltage modulation i.e. the Nyquist curve displays several distinct semicircles.

The individual resistances can be approximated directly from the Nyquist plot, but a more accurate method is to fit an equivalent circuit model to the measured data. The equivalent circuit that is used in this study is shown in Figure 5, more detailed definition and explanation for the model can be found in [14]. The model is clearly quite complicated and thus it requires some simplifications to be reliably fitted to the measured data. Usually it can be assumed that the contact between the photoelectrode and substrate is good which allows replacing the interface resistance and capacitance with short circuit. Similarly, if the cell is illuminated and at open circuit state, the resistance and capacitance between the substrate and the electrolyte is assumed to be very large compared to the other parameters and they can be replaced with an open circuit. The cell is most often measured in open circuit condition where the model can be further simplified by combining the resistances within the TiO_2 film into one R_{PE} and the capacitances of the cell into one constant phase element CPE. With these simplifications, we have a more practical model (Figure 6) [14].

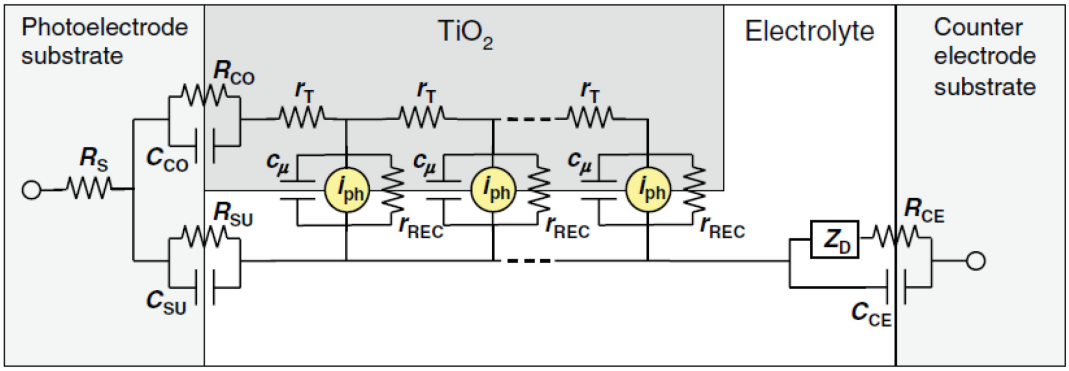

Figure 5 Equivalent circuit model of a DSC. The figure was obtained from [14]. The components shown are the ohmic series resistance of the cell R_S, the TiO_2-substrate contact resistance R_{CO} and capacitance C_{CO}, electrolyte-substrate contact resistance R_{SU} and capacitance C_{SU}, charge transport resistance of the TiO_2 film r_T, recombination resistance r_{REC} and capacitance C_μ, the electrolyte-counter electrode resistance R_{CE} and capacitance C_{CE} and the mass transport impedance through the electrolyte Z_D.

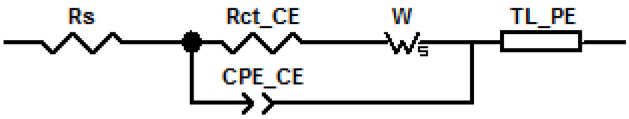

Figure 6 The equivalent circuit after simplifications. The figure is copied from the program Zview that is used for the fitting. W is a Warburg element which corresponds to the transport impedance of the electrolyte and TL_PE is the combined resistances of the photoelectrode.

Before we finish the discussion on the theory of EIS measurements, let us take a closer look on the diffusion resistance of the electrolyte, R_D, as it is very relevant to the results of this work. The R_D is the resistance part of the impedance element Z_D and it can be expressed mathematically as:

$$R_D = \frac{k_B T d}{n^2 q_e{}^2 c_i D_i}. \tag{6}$$

Now k_B is the Boltzmann constant, T is the temperature of the electrolyte, d is the diffusion distance, n is the number of electrons transferred in the overall electrode reaction, c_i and D_i are respectively the concentration and diffusion constant of the species i [14]. As discussed in chapter 2.3.1, the operation of a DSC is often diffusion limited by the concentration of tri-iodide I_3^-. From equation *(6)* we see that the diffusion resistance is inversely proportional to the concentration of the diffusion species c_i (which in this case is replaced with $c_{I_3^-}$), so in addition to introducing the limiting current as discussed previously, the degradation of tri-iodide charge carriers can cause an increase in the diffusion resistance R_D. In IV data of a DSC, this increased resistance is detectable as the decrease of fill factor unless some other reaction affects the fill factor simultaneously. We again did not consider the diffusion of the I^- redox mediator since, as discussed before, its concentration in a DSC electrolyte is much higher than the concentration of the I_3^-.

2.3.3. Incident photon-to-charge carrier efficiency

The incident photon-to-charge carrier efficiency, which is also called incident photon-to-electron conversion efficiency or quantum efficiency (QE), is a parameter that illustrates how well a solar cell converts incoming photons to charge carriers. In other words, it defines the probability at which a photon hitting the photoelectrode is converted into electrical charge in the external circuit [28]. The purpose of IPCE can be easily shown as the amount of generated current:

$$i_{SC} = \int_{\lambda_{min}}^{\lambda_{max}} \Phi(\lambda)\eta_{IPCE}(\lambda)d\lambda. \tag{7}$$

In the above equation IPCE is $\eta_{IPCE}(\lambda)$, incident photon flux is $\Phi(\lambda)$, and the integration limits are the wavelength region under investigation [14].

The IPCE can be further divided into three parts:

$$\eta_{IPCE}(\lambda) = \eta_{LH}(\lambda)\eta_{INJ}\eta_{COL}(\lambda). \tag{8}$$

These components are light harvesting efficiency η_{LH}, electron injection efficiency η_{INJ} and electron collection efficiency η_{COL}. Light harvesting efficiency is a measure of how large share of incoming light is absorbed into the sensitizer dye. It is strongly wavelength-dependent, with shorter wavelength generally absorbing more efficiently. There is also some minimum photon energy, below which the dye will not absorb any photons. This limit and the overall shape of the absorption curve are dependent on the properties of individual dyes. Electron injection efficiency is the probability that an excited electron in the dye is injected into the TiO_2 layer. This process can also be wavelength dependent but generally it is nearly constant over the used wavelength region. Finally, the charge collection efficiency describes the probability of an electron to successfully diffuse through the TiO_2 photoelectrode to the electrical contact. This parameter is also wavelength dependent since the light wavelength affects the absorption profile at the photoelectrode so that light with shortest wavelengths are absorbed mostly close to the surface, and thus have shorter distance to diffuse through which is visible as large collection efficiency [14].

The IPCE measurement is conducted with a monochromatic low intensity light in order to be able to scan the wavelengths separately and to avoid any charge transport limitations of other parts of the cell to affect the measurement. Therefore, it should be noted that phenomena such as electron trapping behave differently than in the case where the cell is fully illuminated because this may cause error if the current is calculated from *(7)*. Since the light used to perform the IPCE measurement has low intensity, effects like the limiting current (see 2.3.1) will not be visible in IPCE data.

An example graph of IPCE data for a DSC with the Z907 dye is shown in Figure 7. The curve has two distinct peaks. The peak around 300 and 400 nm is the direct absorption of UV light by the TiO_2 itself and thus is not related to the properties of the dye. The larger peak at longer wavelengths is the IPCE that is dependent on the dye, and it can have different amplitudes and shapes depending on the dye molecules of the cell. In addition to the absolute IPCE plotted in Figure 7, it is often useful to plot also the relative IPCE, normalized to the maximum, so that differences in the shape of the curves become recognizable.

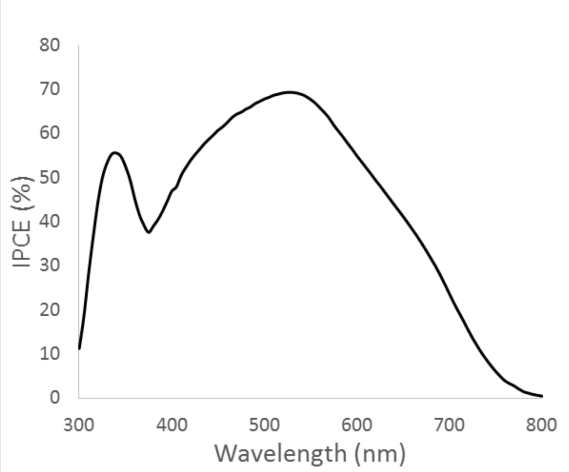

Figure 7 An example IPCE spectrum of a DSC. The two peaks that correspond to the light absorption of the TiO_2 and the dye are clearly distinguishable.

2.3.4. Image processing

Iodine of the electrolyte in a DSC has a very distinct dark yellow or orange color. Therefore, changes within the electrolyte that affect the concentration of iodine can be confirmed visually. These changes can arise from chemical reactions that alter the structure of iodine compounds or from diffusion of iodine to different parts of the cell.

In order to track these changes using quantitative and non-destructive methods, an image processing method has been developed [29]. The method involves taking photographs of each of the cells in accurately maintained conditions. To achieve adequate accuracy, the photographing setup must be protected from any external illumination effects and the illumination must be balanced and constant throughout all of the measurements. Thus, the photographing requires a separate chamber where these variables can be adjusted. The accuracy is improved further by setting the white balance of the camera before each round of measurements and by taking a picture of a calibration color palette, which can be later used to generate a unique color profile for each of the measurements. The pictures are analyzed by selecting an interesting area of the cell (see Figure 8), and computing the average RGB values there. RGB is an 8-bit format used to computationally define colors as a mix of red, green and blue, where each of the three colors is given a value between 0 and 255 to define the saturation of that color. By comparing the RGB values throughout aging process of DSCs, we can track iodine-related changes in the electrolyte. As blue is the complementary color of orange, the changes in iodine electrolyte color are mostly visible as the change of B-component of RGB. Increase of the blue value means that the color of the electrolyte is bleached i.e. it becomes more transparent. It has been shown that the concentration of iodine is linearly dependent on the blue value in concentrations between 0.025 and 0.1 mol/l. In this range, a change of magnitude one in the blue value corresponds to a change of 7.35×10^{-4} mol/l in the concentration of iodine [29].

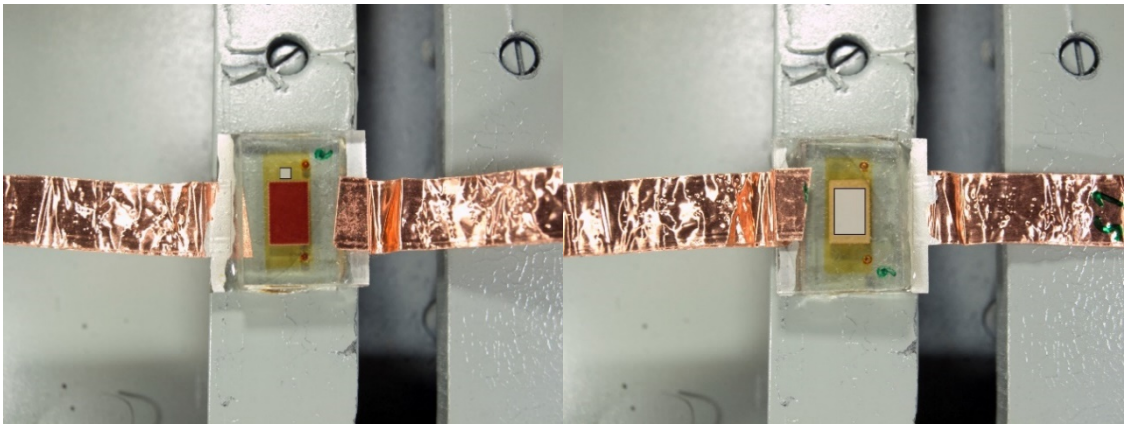

Figure 8 Examples of photographs used in the image processing. The gray boxes on the cells show the area from which the average RGB is calculated. In the left image, the color of the electrolyte is taken with the gray cell stand as a background and on the right the back side of the photoelectrode is the background. By taking the value from two spots, froming of iodine concentration gradients can be detected. The electrolyte RGB value was taken from the top side of the cell since it is generally cleaner.

3. Experimental section

This section describes the materials and methods used in the assembly of the different solar cells. The first chapter (3.1) details the structure of the reference cells, while the changes to this basic structure made for the absorber polymer cells and biomaterial cells are explained in their respective chapters. In addition, the different measurements and the devices used to perform them are detailed here.

3.1. Reference cell structure and assembly

The DSCs configuration used here was so-called sandwich structure where the active components of the cells were sealed between two glass plates. A schematic of this structure can be seen in Figure 1 and a photograph of an assembled cell can be seen in Figure 9.

The glass substrates were made from fluorine-doped tin oxide (FTO) glass (TEC-15, Pilkington). The counter electrode substrates had two small holes to allow the injection of electrolyte into the cell. The glass substrates were cleaned by rinsing them with water, washing detergent, ethanol and acetone. The substrates were also UV treated for 15 min (UV/Ozone ProCleaner™, Bioforce nanosciences) before being used in the assembly process.

The photoelectrode substrates were given a $TiCl_4$ treatment by immersing the glass plates in a solution of titanium (IV) chloride tetrahydrofuran complex (1 w-%) in de-ionized water for 30 minutes in 70 °C. The purpose of the treatment is to decrease the edge potential of the photoelectrode conduction band and decrease the rate of recombination between the electrolyte and electrons in the photoelectrode [30]. TiO_2 photoelectrode itself was printed on the treated substrates with a screen printer AT-60PD, ATMA. The complete TiO_2 layer was formed by printing two layers of paste with small TiO_2 particle size (Dyesol, DSL 18NR-T) and one layer of large, light scattering particles (Dyesol, DSL WER2-0). The resulting photoelectrode was roughly 12 μm thick with an area of 0.4 cm^2. The photoelectrodes were sintered at 450 °C, after which the $TiCl_4$ treatment was repeated, followed by another sintering. The sensitization of the TiO_2 layers was performed by immersing them in a dye solution overnight. The solution used in this study had 0.2 mM of Z907 (Dyesol) in 1:1 solvent of acetonitrile (ACN) and tert-butylalcohol (TBA).

A platinum catalyst layer was formed on the counter electrode by pipetting 4 μl of 5 mM H_2PtCl_6 in 2-propanol on the substrate. The counter electrodes were thermally treated in 390 °C for 20 minutes.

The basic electrolyte that served as a template for all of the other electrolytes had been prepared and purified for an earlier work [31]. The electrolyte consisted of 0.5 M NMBI, 0.5 M PMII, 0.1 M GuSCN and, after adding more iodine, 0.1 M I_2 in MPN.

The cells were assembled by melting a frame foil cut from Surlyn® 1702 ionomer resin film (20 μm thickness, DuPont) between the substrates and then pressing the electrodes together. Then, in the case of liquid electrolytes, the electrolyte was injected through the holes in the counter electrode, which were sealed by melting another layer of Surlyn® with a microscope glass. Contacts were made by attaching copper tapes to the electrodes and then the electrical contact was improved with a layer of silver ink (SCP, Electrolube) between the

substrates and the copper tapes. Finally, the mechanical durability of the cells was enhanced with a layer of epoxy glue on top of the contact. Many of the tested modified electrolytes were inserted into the cells using other techniques than injecting which will be discussed in their respective chapters.

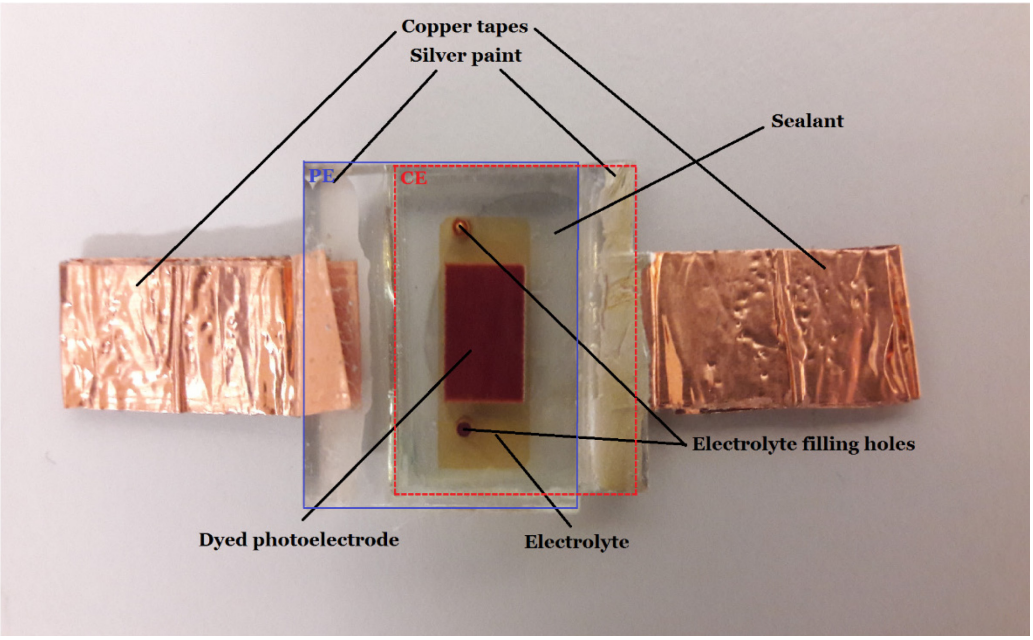

Figure 9 A photograph of an assembled DSC. The different components described in the chapter above are marked. Also the glass substrates of the photoelectrode (PE) and counter electrode (CE) are marked with blue and red outlines, respectively. The photoelectrode is on top of the counter electrode.

3.1. Experimental details of effect of external circuit state on the aging of dye solar cells

A series of 27 similar DSCs with only the same type liquid electrolyte was assembled (by injecting the electrolyte) and separated into three groups of nine cells each. After the assembly and before the initial measurements all of the cells were stabilized in 1Sun light soaking overnight. During the aging proper, one of the groups was aged in open circuit condition while in another group the cells were short circuited. The cells of the last group were placed into a simple circuit with a resistor load of 120 Ω, which was close to the load required for the cells to be in their initial maximum power point: 110±5 Ω. The resistance required by the maximum power point was calculated simply with the Ohm's law at the maximum power point:

$$R_m = \frac{V_m}{I_m}. \tag{9}$$

All of the cells were aged under constant 1Sun illumination for 1080 hours. During the aging, the cells were protected with a UV filter (cut-off at 400 nm wavelength, SFC-10 clear, Asmetec). The degradation of the cells was monitored with weekly measurements of the IV curves, open circuit EIS and photographs of the cells. Additional measurements performed before and after the aging included IPCE, short circuit current dependence on intensity and transmittance

of the electrolyte. Few cells from each of the different groups leaked or demonstrated other anomalous behavior during the aging, and were thus excluded from the analysis. This aging test was performed with the lamps presented in Figure 13, since it corresponds more closely to the actual solar spectrum. The UV light was cut off with the UV filter to minimize the effect of UV light on the cell degradation, allowing the study to focus on the effect of the circuit state. The use of the UV filter is justified since it is cheap, thin and flexible. As such, it could be incorporated to the commercial cell structure itself.

3.2. Experimental details of polymer impurity absorbers

The goal behind using polymer impurity absorbers is twofold: firstly, absorbing harmful impurities, most notably water, which increases the stability of the cell and secondly changing the state of the electrolyte into semi-solid, which would make the mass production of DSCs easier than in the case of liquid electrolyte. Three different polymers were tested as impurity absorbers within the electrolyte of the DSCs: Poly(methyl methacrylate) (PMMA), Polyvinylpyrrolidone (PVP) and Polyacrylic acid (PAA). Of these, PMMA is capable of absorbing the smallest amount of water (0.3-0.4 w-%) [32] and therefore it was used as a reference to indicate whether the addition of a relatively inert polymer has an impact on the performance of a DSC. PVP has both hydrophilic and hydrophobic functional groups, which makes it able to interact with various different substances and makes it soluble in a large variety of solvents. PVP is capable of absorbing roughly 40% of its weight of water [33]. In theory PVP could be dissolved to the electrolyte of a DSC, where it could absorb any excess water. PAA is capable of absorbing even larger amounts of water, holding many times its original volume of water [34]. Other attractive properties of these polymers are their price, good commercial availability and safety. For example, PAA is used as absorber in disposable diapers and PVP as a binder in pharmaceutical pills, passing harmlessly through human digestive system. The chemical composition of the polymers is shown in Figure 10. The tested materials were provided by Dr. Jaana Vapaavuori, Tampere University of Technology / University of Montreal, along with the idea of testing these materials.

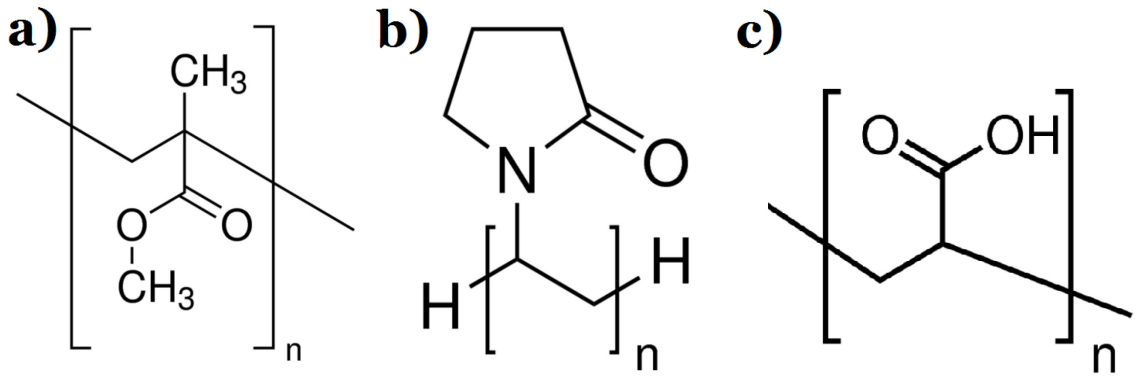

Figure 10 Chemical structures of a) PMMA, b) PVP and c) PAA [35].

All of the polymer powders were dried in a vacuum oven at 80 °C overnight before being used in the cells. Different cell assembly methods were required for different polymers: PMMA was simply dissolved to the electrolyte, which was

then injected into the cell as in the liquid reference cells. PAA did not dissolve into the electrolyte, so it was mixed to 2-propanol and drop-cast on the counter electrode. The 2-propanol solvent was evaporated on a hotplate in 120 °C before assembly. In the case of PVP, both of the aforementioned methods were utilized to study if there are any mentionable differences between them. The electrolyte used in the polymer absorber studies was otherwise similar to the basic electrolyte described in 3.1, except for GuSCN, which was left out from all of the cells due to apparent chemical incompatibility with PVP (Figure 11). This test series was aged under UV light, since it is hypothesized (chapter 2.2) that UV light enhances adverse effects of water within the cell. As the absorbers were designed to improve cell stability against water, UV stability test should highlight beneficial effects of the impurity absorbers. In the work of Tiihonen et al., it was also noted that the degradation of the cells appeared to be directly related to the amount of UV light and basically irrespective of incident visible light [36]. Having a high amount of UV light can thus be used to accelerate the aging test even further. Due to the fast degradation usually caused by UV aging, the cells were monitored by measuring them several times in a week. The cells were aged in open circuit since the study was focused on the effects of the different absorbers on the cell performance and lifetime. By aging in open circuit, any additional degradation mechanisms caused by the state of the circuit were avoided. The effect of the external circuit is discussed in chapter 4.1.

The absorber polymer cells were assembled in two groups: first one was used mainly as a practice to find out the necessary methods for assembling cells with each of the polymers. For example, this was how the method to drop-cast PAA on the cell was decided, since PAA was not soluble in the electrolyte. Due to the results obtained during the first test series, PMMA cells were not assembled at all for the second group of cells (see chapter 4.2 for more information). Naturally, both of the groups had their own reference cells.

Figure 11 Polymer PVP reacted with GuSCN by forming a mass of white lint. For this reason GuSCN was left out from the electrolyte used in this series of tests.

3.3. Experimental details of biomaterial aerogels

The use of biomaterial aerogels had a main goal of improving cell assembly and mechanical stability: by placing the aerogel membrane on the photoelectrode and then soaking it with liquid electrolyte, the electrolyte could be held in place before the cell was sealed, eliminating the need for injection, which would simplify mass production and possibly increase cell lifetime. Four different bio-aerogel films were tested here: bacterial cellulose (BC), Nano-fibrillated cellulose (NFC), Tempo-nano-fibrillated cellulose (TEMPO) and Chitin. In practice, all of the cellulose materials used here are networks of cellulose nanofibers, only the different production methods cause differences in the properties of the resulting films. NFC is created from a cellulose source material, such as woodpulp, using one of several possible top-down methods. TEMPO cellulose is created similarly, but is additionally pretreated with TEMPO-oxidation to facilitate enhanced separation of nanofibers. In contrast to the previous ones, BC is created using bottom-up method where gluconobacteria are used to grow the cellulose nanofibers. The film grown by the bacteria is then freeze-dried to obtain an aerogel [37]. Chitin is similar in structure to cellulose but instead of wood, it can be extracted for example from shrimp shells. The aerogels used in this work were prepared by and received from D.Sc. Maryam Borghei and M.Sc. Janika Lehtonen of the Department of Forest Products Technology, Aalto University. The thickness of the aerogels was in the range of 50 µm. SEM images of the prepared aerogels can be seen below (Figure 12). Pieces of aerogel were cut for use within the cells with an Epilog 35W Zing-laser scriber.

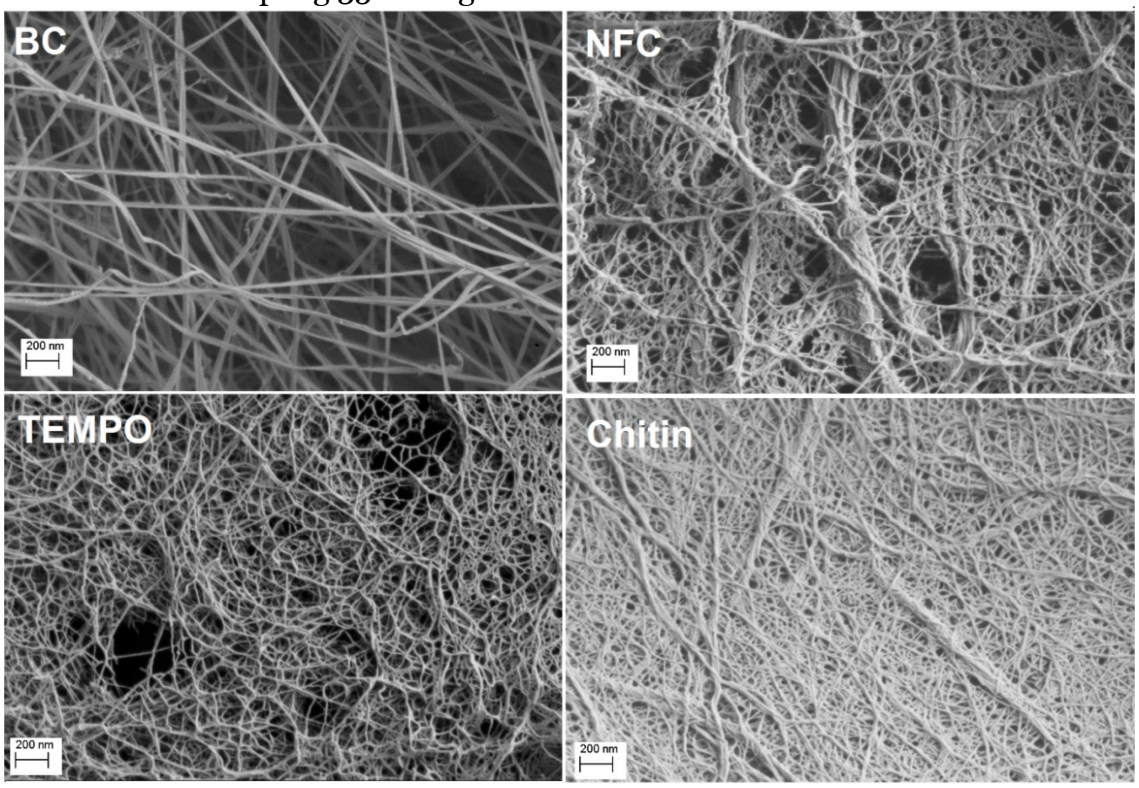

Figure 12 SEM images of the bio aerogels used in this study. Images were received from D.Sc. Maryam Borghei. Scale bar at the lower left corner of the images is 200 nm.

For the study, five groups of DSCs were assembled. One group of reference cells without any aerogels within the cell, and four test groups: one for each of the different aerogels. As in the case of impurity absorbers, the aerogels were dried

in a vacuum oven at 80 °C. The cells were assembled by first attaching the Surlyn frame foil to the counter electrode by heating it on a hotplate pressed against a Teflon piece. The aerogel was placed on top of the dyed photoelectrode then 3.5 µl of electrolyte was dropped on it with a micropipette. The electrolyte spread evenly to the aerogels and there was only minimal leakage to outside of the aerogel. Finally, the cell was sealed by pressing the counter electrode with the attached Surlyn foil against the photoelectrode on a hotplate. Naturally, there were no holes for the electrolyte injection in the counter electrode substrates. In order to have enough space to fit the aerogels inside the cells, two frame Surlyn foils were stacked increasing the distance between the electrodes to about 50 µm. The reference cells were assembled as described in 3.1, except the amount of injected electrolyte was the same 3.5 µl as for the aerogel cells to keep the cell groups comparable. The bio-aerogel cells were aged with the UV aging system. This aging method was chosen due to promising initial results and time limitations (UV aging tends to last for a shorter time). This is also the reason why the IV measurements of the cells were performed three times in a week to monitor their faster degradation. As in the case of absorber polymer cells, the aging was performed in open circuit to avoid any of the additional degradation mechanisms discussed in chapter 4.1.

3.4. Measurements

The cells were characterized using multiple different measurement techniques that reveal several details of the operation of DSCs. IV measurements for the solar cells were performed with a Peccell PEC-01 solar simulator. The simulator utilized a xenon lamp that produced a simulated 1000 W/m² sunlight with a good match to the standard AM1.5G-spectrum. The light was calibrated with a PV measurements Inc. Si KG5 photodiode. The cells were measured in room temperature and they were covered with tape masks in order to prevent reflected light from affecting the measurement. The potentiostat was a Keithley 2420 3A Sourcemeter. The set voltage range for the DSC measurements was from -0.3 V to 0.8 V with a step size of 0.01 V and a delay of 0.1 s before logging each data point.

Incident Photon-to-Charge Carrier Efficiency (IPCE) was measured with QE/IPCE Measurement system QEX7 (PV Measurements Inc.). The used wavelength range was 300 nm to 1000 nm, without bias light.

Transmission of light through the electrolyte of the cells was studied with OceanOptics USB2000-XR1-ES spectroradiometer. The wavelength range here was roughly from 200 nm to 1000 nm.

Changes in short circuit current of the cells as a function of incident light intensity was also studied. This measurement was performed for DSCs in initial state and after they had been aged for 1000h. The goal of these measurements is to accentuate the changes of limiting current between fresh and aged cells. This measurement was made with an in-house built device: Automated Variable Intensity Measurement Unit (AVIMU), which used four LXML-PWC2 Cool White LUXEON Rebel ES LEDs to illuminate the cells one by one with different intensities. The power into the LEDs was varied so that the range of illumination intensity varied between 0.4 to 9 times the intensity of 1Sun illumination. The IV curves were measured from 0.2 V to -0.8 V with a step size of 0.02 V on several illumination intensities with an Autolab PGSTAT T302 potentiostat.

Electrochemical Impedance Spectroscopy (EIS) measurements were performed with a Zahner Zennium potentiostat. The used AC frequency range was from 4 MHz to 100 mHz. The measurements under illumination were performed in open circuit conditions. The amplitude in the measurements was 10 mV. Fitting of the equivalent circuit model to the data was done with ZView2 (Scribner Associates, Inc.).

An Olympus E-620 camera was used to photograph the cells weekly for the image processing measurement, where chemical changes within the cells were studied optically. The photographing setup was covered from all sides with a black canvas to prevent ambient light from affecting the measurement. The camera was attached to a movable tray, which also had four LED lamps to provide well-controlled illumination of the photographed cells. The white balance was defined using the camera's own functionality and the color profile for the pictures was set in Adobe Lightroom3 with the help of a color checker passport (X-Rite). The pictures were also converted from RAW to JPEG while the color profile was defined. The average RGB values were calculated from the photographs with MatLab® by selecting a small area from the cells for analysis.

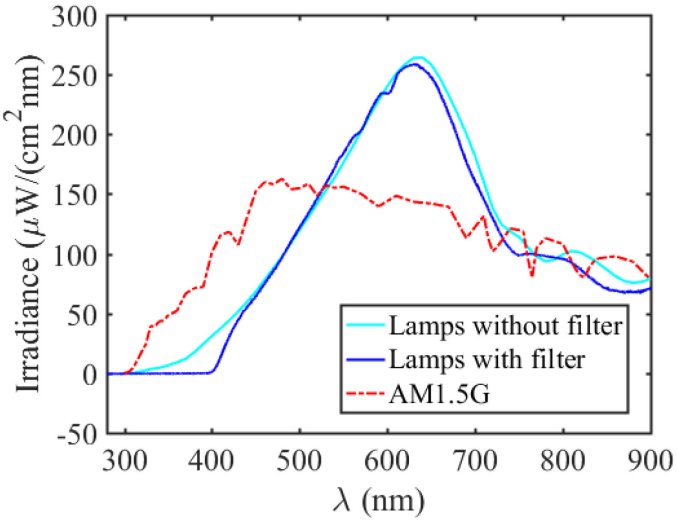

Figure 13 The standard spectrum of AM1.5G and the spectrum of the lamps used in the aging tests with and without UV cut-off filter. The effect of the cut-off filter can be clearly seen at 400 nm wavelength. Even without the filter the amount of UV light is clearly lower than in the reference solar spectrum and thus a separate system was used to test the UV stability.

The 1000h aging of the cells was performed with an in-house built system that had eight Philips type 13117 halogen lamps. The system produced roughly a 1Sun illumination on the area the cells were placed on. The cells were protected from UV light with a UV cutoff-filter placed between the cells and the lamps. The spectrum of these lamps with and without the UV filter is compared with the AM1.5G spectrum in Figure 13.

The UV aging was performed in a weather cabinet Arctest Arc-150. The temperature of the cabinet was set to 12 °C, which resulted the in a temperature of 50 °C for the cells. The difference in the temperature was caused by the heating effect of the UV lamp, which was an Osram Ultra-Vitalux 300 W. The cells in UV tests were aged in open circuit conditions. The spectrum of the lamp had 1.5 times the amount of UV light as the 1Sun standard but in the visible region there was only about 34% of the 1Sun intensity. The comparison between the spectra is shown in Figure 14.

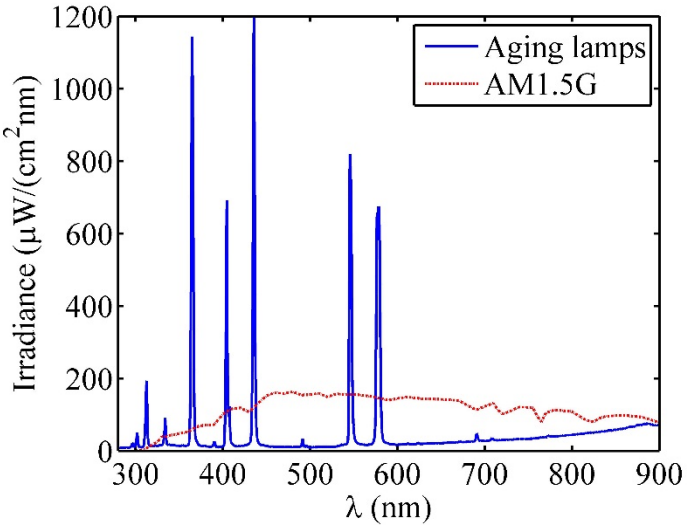

Figure 14 The standard spectrum of AM1.5G and the spectrum of the lamps used in the UV aging. The lamps clearly emit only on certain wavelengths and in the infrared, while the solar spectrum is more even. [38]

4. Results and discussion

Here the results from the different tests are presented and discussed in separate sections.

4.1. Effect of external circuit state on the aging of dye solar cells

The aging for 1000h was completed successfully for the cells aged in different circuit states. As expected, the initial performances of all the assembled cells were similar since the cell structure was identical and differences arose only during the aging. For comparison, the IV curve of one typical cell from each of the groups is plotted before and after the aging in Figure 15. The average numerical values of the cell parameters are collected to Table 1 and the development of these values as a function of time is illustrated in Figure 16. The cells that were designated to each of the aging groups were selected so that each of the groups has similar distribution of initial performances. Of course, as can be seen from Table 1, the variations between the initial cell parameters were small anyway.

The quickest changes in the cells during the 1000 h aging without UV light occurred between the first two measurements, i.e. during the first four days of aging. In that time the open circuit voltage of all cells decreased slightly, the exact amount depending on the state the cells were aged in. The voltage decreased least in the cells in open circuit and most in the short circuited cells. In addition, the fill factor decreased during the initial aging: in open circuit- and load cell groups the fill factor was lowered only by few percentage points from the initial 0.6 but for the short circuit cells the average was decreased all the way to 0.5. This had an instant effect on the efficiency of the cell groups and the performance of short circuit cells was already clearly separated from the other cell groups. After these initial changes, the rate of aging slowed in all of the cells. Fill factor remained almost constant and the rate of degradation of the open circuit voltage was very slow. Short circuit current did not change either. So all of the cells remained relatively stable until around 350 h the short circuit current I_{SC} of the cells aged in short circuit began to decrease rapidly. The open circuit voltage was still decreasing at the same rate as previously in all of the cell groups. The rapid decrease of short circuit current did not have a large impact on the rate of change of the efficiency of the short circuit aged cells, since as their current started to decrease, their fill factor began to increase. This countered the loss of performance from the lowered short circuit current to some degree. It is possible that the decrease of the short circuit current was caused by the degradation of significant amount of the charge carriers in the electrolyte. This would cause less current to be transported through the electrolyte but also decrease recombination losses from the photoelectrode to the electrolyte, increasing the fill factor. It would explain why the decrease in short circuit current did not begin immediately at the start of the aging: the iodine electrolyte is mixed with an excess amount of charge carriers. Thus, at the beginning, the performance of the cells would not be limited by the charge transport through the electrolyte, but if the charge carriers were to degrade during the aging, the cell operation would become limited by the charge transport of the electrolyte. This hypothesis will be studied and discussed

further in the analysis of other measurements. There were no more changes in the degradation rates of the cell parameters for the rest of the aging.

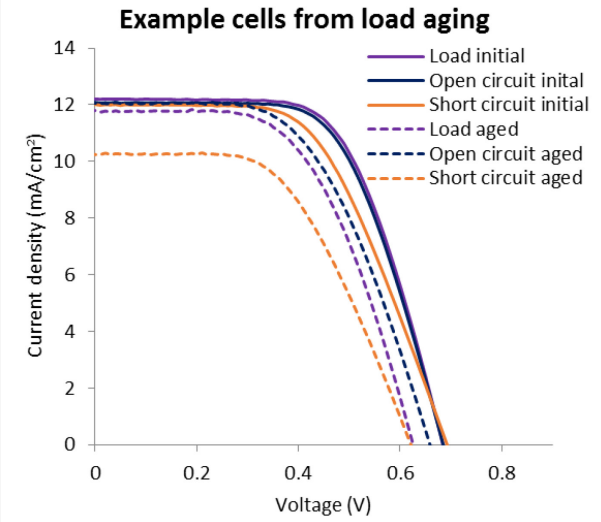

Figure 15 IV curves of example cells before (solid lines) and after (dashed lines) the aging. The selected cells were as close to the average cell as possible.

Table 1 Average and standard deviation of cell parameters before and after the aging. The R_{cell} in the final column is the total resistance of a cell when in short circuit.

External circuit	State	I_{SC} [mA/cm²]	V_{OC} [mV]	*FF* [%]	Eff [%]	R_{cell} [Ω]
Load	initial	12.4 ± 0.2	685 ± 3	60 ± 3	5.0 ± 0.3	41.0 ± 7.7
	1080 h	11.5 ± 0.3	634 ± 8	56 ± 3	4.2 ± 0.2	42.2 ± 6.1
Open circuit	initial	12.2 ± 0.2	686 ± 3	62 ± 2	5.2 ± 0.2	36.6 ± 3.5
	1080 h	11.6 ± 0.9	652 ± 4	56 ± 4	4.2 ± 0.3	44.0 ± 7.3
Short circuit	initial	12.1 ± 0.3	688 ± 6	60 ± 4	5.0 ± 0.2	41.2 ± 7.2
	1080 h	10.1 ± 2.2	620 ± 20	54 ± 8	3.2 ± 0.3	50.3 ± 6.2

In the end, the aging of the cells in open circuit and under load performed very similarly. There was a small difference in the open circuit voltage of the groups throughout the aging, but it was not large enough to really affect the other cell parameters. The final average efficiency of both cell groups was 4.2%. The cells aged in short circuit were clearly separated from the other two groups. Due to the faster degradation of the short circuit current, these cells ended the aging with an efficiency of 3.2%. Curiously, the current did not decrease as quickly in all of the short circuit cells as can be witnessed by the large deviation, but this was compensated by lower fill factor in those cells so that all of the cells reached similar final efficiencies.

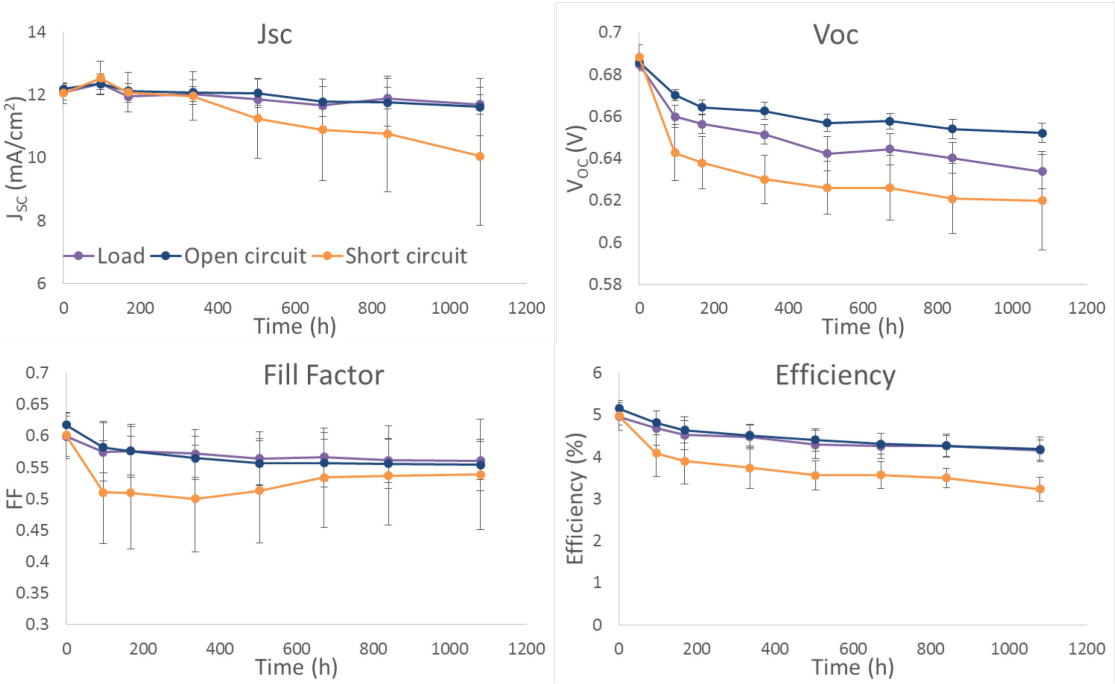

Figure 16 The averages of different cell parameters obtained from the weekly IV measurements.

To see if the effect of limiting current influenced the degradation of cell performance, I_{SC} was measured as a function of the cell illumination intensity. If short circuit current of a cell does not increase notably when the illumination intensity is increased, the current of the cell is likely affected by the limiting current (see 2.3.1 for more detailed explanation). The intensity of light was varied from 0.35 to 9 Sun equivalents. The measurements were performed before and after the aging. The results of the measurements are plotted for each of the groups separately in Figure 17.

As expected for similar cells, the current-intensity-behavior of all of the cells were nearly identical initially: at lower intensities the short circuit current followed the illumination intensity linearly. When the intensity reached about 3 Sun equivalents, the current began to increase at a slower rate compared to the earlier, linear rate. After the aging, the cells aged under load and in open circuit performed similarly to the initial measurement results. At lower intensities the currents were very similar to the initial values and the dependence was once again linear but at high intensities, after around 3 Suns again, the increase rate became even slower than initially. Overall, the shape of the current-light intensity curve was similar initially and at the end of the measurement for the load and open circuit cells, allowing the assumption that the limiting current did not significantly affect the cell performance in those cases. For the cells aged in short circuit the situation is different however. The aging clearly affected the intensity response of the short circuit cells: their currents were significantly lower than initially already under 2 Sun illumination, and in the case of the worst cells the difference was visible already at 1 Sun illumination, with currents about half of the originals. The aged short circuit cells are split in two groups: there appears to be 10 mA/cm² difference between their current values but otherwise their behavior is similar, i.e. their current increases at a similar rate as a function of the light intensity. All of these cells are however far from the initial case when considering that the data is plotted on a logarithmic scale.

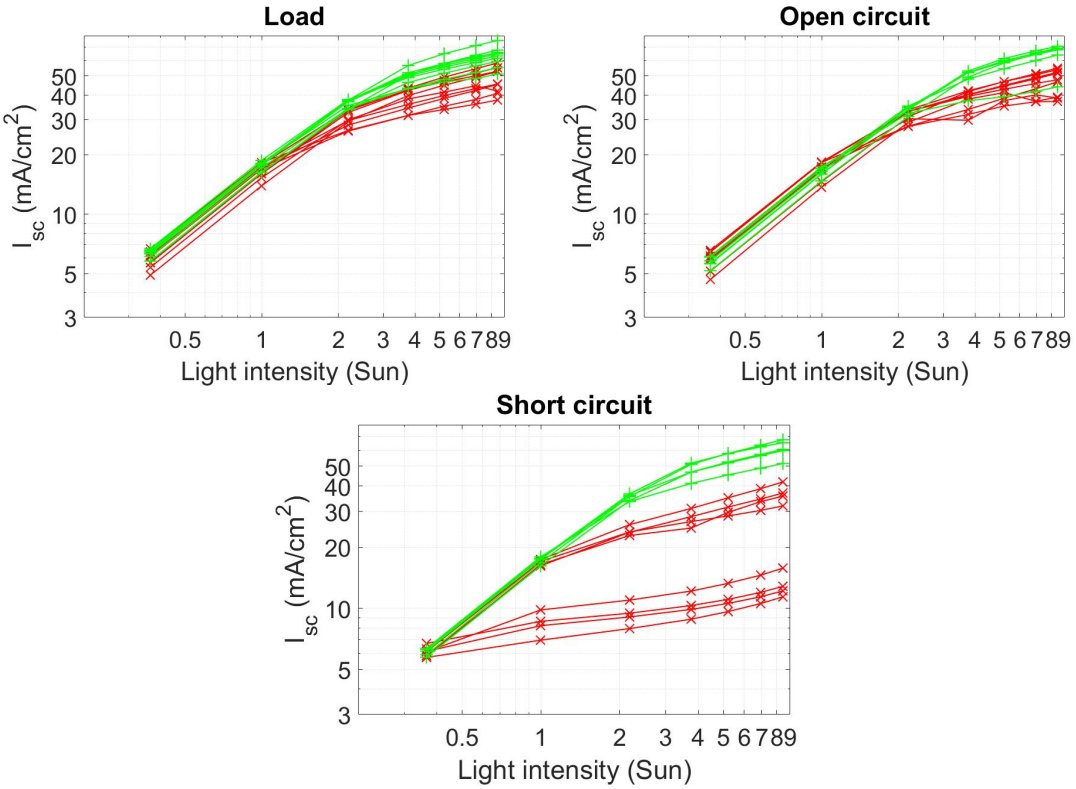

Figure 17 The dependence of I_{SC} on the incident light intensity. The measured value for each of the separate cells is shown in the plots, with green curves indicating initial state and red curves for the aged cells.

The reasons for the large variations in the currents of the aged short circuit cells are not immediately clear. Such results could be caused by differences in light intensity during the aging. The intensities were however monitored when the weekly measurements were performed, and the intensity variation was too small to warrant such a large deviation in the cell performances. A more likely explanation is that the short circuit of some of the cells was not as perfect as in others, resulting in a larger resistance between the electrodes of the cell through the external circuit which caused decrease in the current flowing through the cell. Cells with less ideal short circuit would be closer to the cells aged under load, although their resistance was still far from the resistance needed for a maximum power point aging. Even if the higher resistance slowed down cell degradation, the aging behavior of those cells was still closer to the better short circuit cells. The differences in the quality of the short circuit can arise from several factors. As the short circuit was formed simply by connecting the copper tapes of opposite electrodes with an alligator clip, the quality of the connection could vary greatly. In addition, the contact between the copper tape and the substrate could play a role in this. It is also possible that the differences between short circuit cells are caused by some completely different phenomenon, such as impurities that may have ended up in some of the cells during assembly, or by a combination of multiple aforementioned factors.

Overall, even the best short circuit cells diverge from the initial cases already at lower light intensities, resulting in clear differences between initial and aged cases. Therefore, cells aged at short circuit appear to be strongly affected by the limiting current i.e. the charge carriers in their electrolytes seem to be degraded.

The IPCE results highlight changes in the photoelectrode performance. Figure 18 displays the initial and aged IPCE spectra for all of the cells aged in

different circuit states. Below the plots of the absolute IPCE are shown normalized spectra, where value 1 was assigned to the maximum of the IPCE above 400 nm wavelength. As can be seen from the normalized curves, the aging had very little effect on the relative shape of the IPCE of the cells, aside from some shifts around the wavelength of 400 nm. This effect was especially visible in the cells aged in short circuit, in which case the IPCE increased roughly 10 percentage points at wavelength 400 nm. This effect has been contributed to the bleaching of electrolyte: as the electrolyte becomes more transparent, it will not absorb as much light on shorter wavelengths thus allowing more light to reach the photoelectrode and generate current [36].

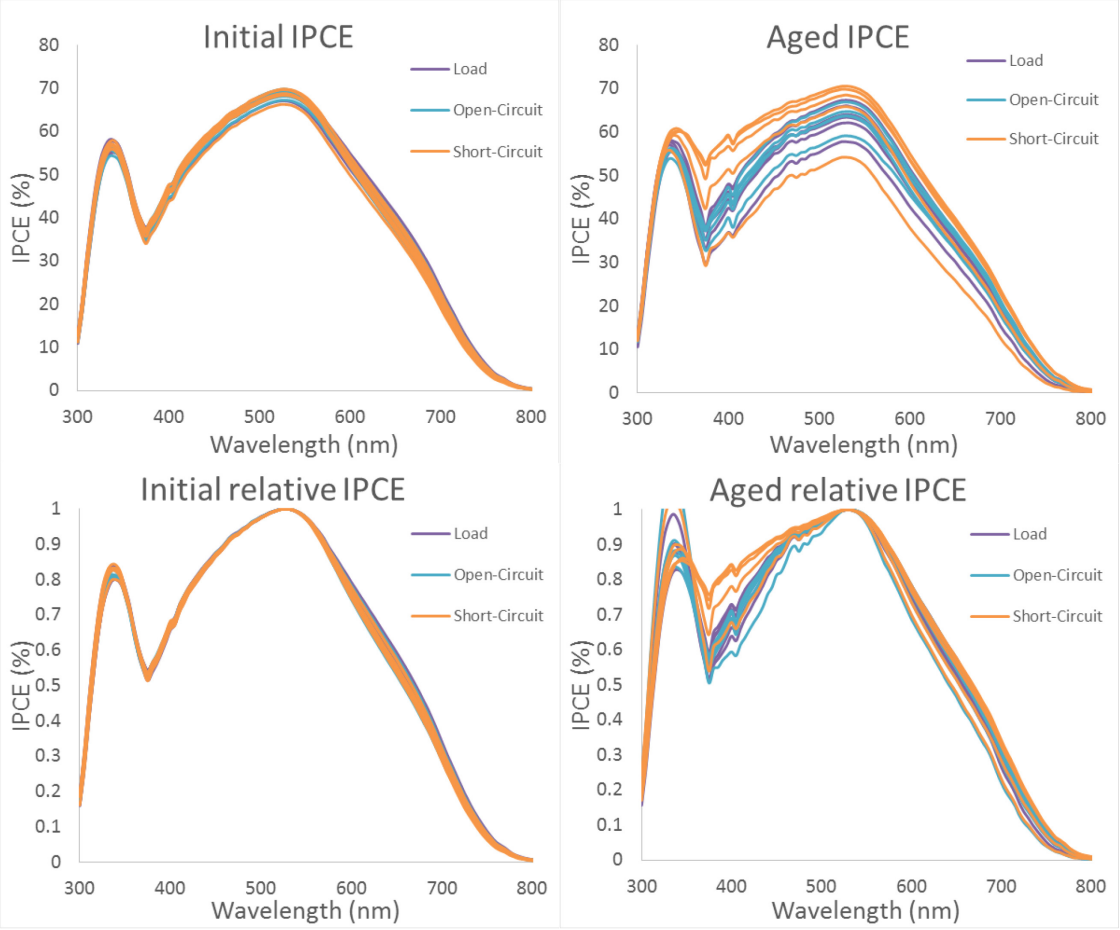

Figure 18 Incident photon-to-charge carrier conversion efficiency curves of the cells from the external circuit status aging test. The plots on the left illustrate the initial status of each of the cells and the figures on the right are the results after the aging. The figures above show the measured values of IPCE while the figures below show the relative curves, where the maximum value (above 400 nm) is set as 1. The relative graphs are useful in detecting differences in the shape of the curves.

The aging also caused a notable variation in the height of the dye absorption peak of the IPCE (the larger peak around 550 nm). The maximum IPCE in that region varied between 50% and 70% for all of the cell groups. Since the smaller, TiO_2 peak was not affected, the variation is likely not caused by changes in the injection efficiency η_{INJ}, which should show only minor dependence on wavelength. Thus the variation would be visible also in the TiO_2 peak. Only remaining options are that either the collection efficiency η_{COL} or the light harvesting efficiency η_{LH} of the dye has decreased in some of the cells during the aging. This effect seems to be independent of the state the cell was aged in, since the average IPCE maxima of the cells are not separated by the aging group,

instead being mixed seemingly randomly. The variation is however clearly highest in the short circuit cells. It is difficult to determine the exact cause for this variation; one possible reason is that some impurities found their way into some of the cells during the cell assembly, causing faster dye degradation during the aging. Small shifting of the overall IPCE during the aging is typical in DSCs, which can be seen for example from the other IPCE results of this study. Overall, this variation did not result in significant differences in cell performances as can be seen from the IV data above and it could be said that the IPCE of all of the different cells was relatively stable during the aging.

The EIS measurements provide extensive information on the internal parameters of the cells (see 2.3.2). The EIS under 1Sun illumination was measured on a weekly basis to monitor the effects of aging on the cells. The initial and aged Nyquist curves of an example cell aged in short circuit are shown in Figure 19. The case shown in Figure 19 is typical for the aging of DSCs. Usually one or more internal resistances are increased during an aging study, which is visible as an increased size of some of the semicircles of the Nyquist plot. The increase of the total resistance, in this example from 31 Ω to 41 Ω, is detected as a decrease of the overall cell performance.

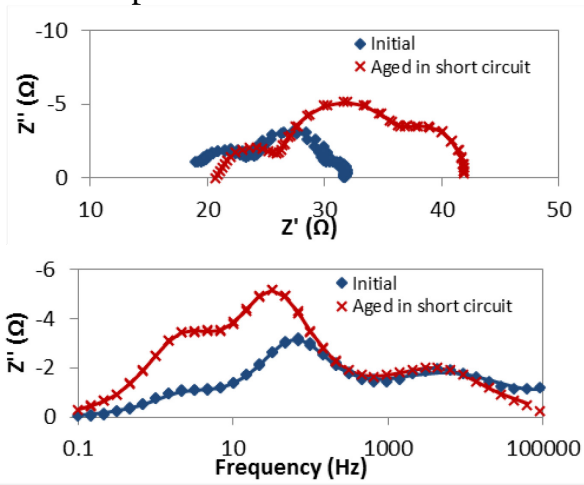

Figure 19 A nyquist plot (left) and a Bode plot (right) of an example cell that was aged in short circuit. Blue curves are measured from the cell in its initial state and the red curves are obtained after the 1000h aging. The markers in the figures are the measured data points and the solid line is the equivalent circuit fit to the data.

The evolution of the total ohmic resistance *Rs*, the electrolyte-counter electrode charge transfer resistance R_{CE} and the diffusion resistance of the electrolyte R_D during the aging are displayed in Figure 20. The behavior of the ohmic resistances *Rs* was similar in all of the cell groups throughout the aging. Between the initial state and the first aging measurement, the *Rs* increased from about 14 Ω to between 20 Ω and 25 Ω. After this initial jump, the ohmic resistances stabilized and remained constant for the rest of the aging. This initial increase of *Rs* is reflected on the IV results of the cells as a similarly sudden decrease of the fill factor and open circuit voltage (Figure 16). It is clear that the first few days of aging caused changes in all of the cells, which collectively increased the ohmic resistance. As almost every component of the DSC contributes to the total *Rs*, it is difficult to single out the exact source. Possible causes range from changes in the sheet resistance of the substrate to the degradation of the electrical contacts, such as the silver paint between the conductive substrate and copper tapes.

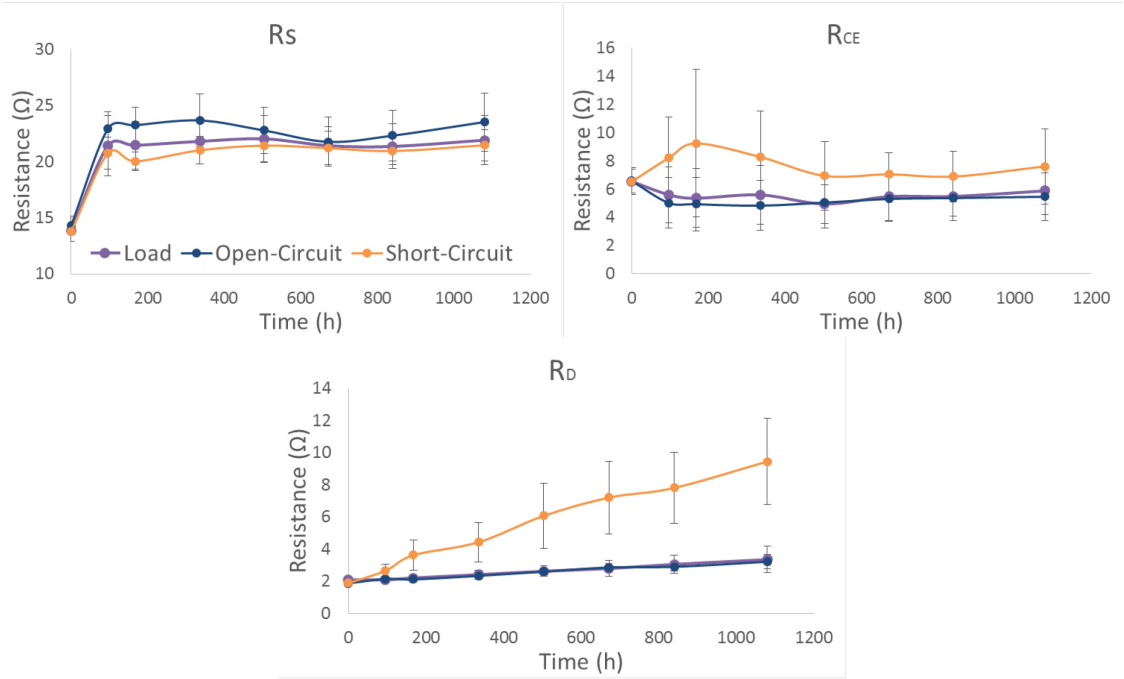

Figure 20 The EIS-measured and fitted internal resistances of the cells. The solid lines display the averages for each of the cell groups and the error bars signify the standard deviation. The displayed parameters are ohmic series resistance (R_S), charge transport resistance at the counter electrode (R_{CE}) and the diffusion resistance of the electrolyte (R_D).

The interfacial resistance R_{CE} remained relatively constant during the aging. Initially the R_{CE} was increased for the short circuit cells by about 4 Ω and decreased by 2 Ω for the others. After 200 hours of aging, the R_{CE} began to trend back to its initial value for all of the cell groups. As a result, the final values of R_{CE} were close to where they were in initial state of the cells. Moreover, the deviations in the values of interfacial resistance R_{CE} were of the same order as these changes. Thus, the values of R_{CE} remained stable in all of the cell groups in a statistically significant sense.

The diffusion resistance of the electrolyte R_D demonstrated the most obvious difference between the cell groups. Initially it was very low for all of the cell groups, only 2 Ω. In the case of the open circuit and load-aged cells, the R_D remained very close to the initial value, linearly increasing to roughly 3 Ω over the 1080 h of aging. In other words, the diffusion resistance remained stable in cells aged at open circuit or under load. The situation is clearly different in the case of short circuit cells, for which the R_D began to increase at a much higher rate immediately after the aging was started. The increase was linear and the average value of R_D in the short circuit cells reached 9 Ω at the end of the aging. There was also larger variation in the values, as is common when some parameter changes significantly. It is clear that aging DSCs in short circuit immediately causes harmful reactions in the electrolyte, which decrease its capability to transport charge. One possible reason for the increase of the R_D can be seen from the expression *(6)*, which is inversely dependent on the concentration of the iodine redox mediators. If the amount of iodine were decreased through some mechanism, the value of R_D would increase [39]. This would suggest that the amount of redox mediators is decreased faster in short circuited cells than in a cell in open circuit or under load. The possible causes for the faster decrease of redox mediators in short circuit is discussed later in this chapter.

The EIS data of some of the cells behaved unusually by displaying a fourth semicircle in the Nyquist plot. This semicircle appeared between the ohmic series resistance *Rs* and the interfacial resistance R_{CE} and varied greatly in size. It became visible only when the voltage fed to the cell was varying on the highest frequencies, namely around 1 MHz. An example is shown in Figure 21. As the aging progressed, the fourth semicircle disappeared from many of the cells. This fourth semicircle has been contributed to be caused by the interfacial resistance between the conducting substrate and TiO_2 layer R_{CO} [40], but as it lacks an established physical model there could be more phenomena involved [14]. In this study, the equivalent circuit fit was made by assuming that the fourth semicircle is caused by the R_{CO}. The causes for the appearance of these semicircles have been discussed in previous work, where the reason was tracked to insufficient rinsing of the glass substrates after the $TiCl_4$-treatment [41]. If the $TiCl_4$ were not rinsed away well enough, the formed compact layer of TiO_2 would be too thick which would increase the interfacial resistance. Discussions with Dr. Ghufran Hashmi during this work indicated a different reason: the fourth semicircles also appeared when the glass substrates were not cleaned thoroughly enough before the cell assembly was begun. Impurities that remained on the surfaces of the glasses from their manufacturing and transport seemed to increase the interfacial resistance. It is likely that both of these are viable explanations to the phenomena, since both have properties that would hinder charge transport to the substrate. The fourth semicircle was not included in the analysis above, since it was visible only in some of the cells and even disappeared from some of those during the aging. The magnitude of the fourth semicircle varied between 1 Ω and 9 Ω, and could both increase and decrease during the aging in those cells where it did not disappear completely. Furthermore, as there is no established model to explain how the semicircle is formed, information gained by including it to the analysis would have been limited.

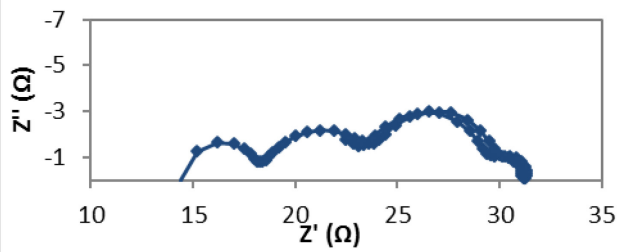

Figure 21 Example of a Nyquist plot from a cell with a fourth semicircle. The extra semicircle is the first from the left and is detected on very high frequencies (around 1 MHz) of the AC current. This curve was measured from an initial cell.

Further proof that the decrease in performance of the cells aged in short circuit was caused by the degradation of charge carriers is obtained by combining results from two of the previously presented measurements. When comparing the short circuit currents of the cells as a function of illumination intensity, it was noticed that there was a large variation in the I_{SC} of the short circuit cells. Similarly, while the diffusion resistance R_D increased in all of the short circuit cells, the variation of the diffusion resistance was large. By comparing these two parameters, i.e. diffusion resistance and limiting current, for each of the individual cells, we can detect if there is any correlation between their magnitudes. The R_D and I_{SC} at 9Sun condition of the short circuit cells after aging is plotted in Figure 22. It is clear that there is a dependence between these parameters. According to equations *(6)* and *(4)*, diffusion resistance and limiting current are both linearly dependent on the concentration of charge carriers in the

electrolyte. Thus, since there is a clear correlation between the limiting current and diffusion resistance, the results indicate that the performance of the short circuit cells is indeed diffusion-limited. In other words, it appears likely that the charge carriers of the electrolyte have degraded.

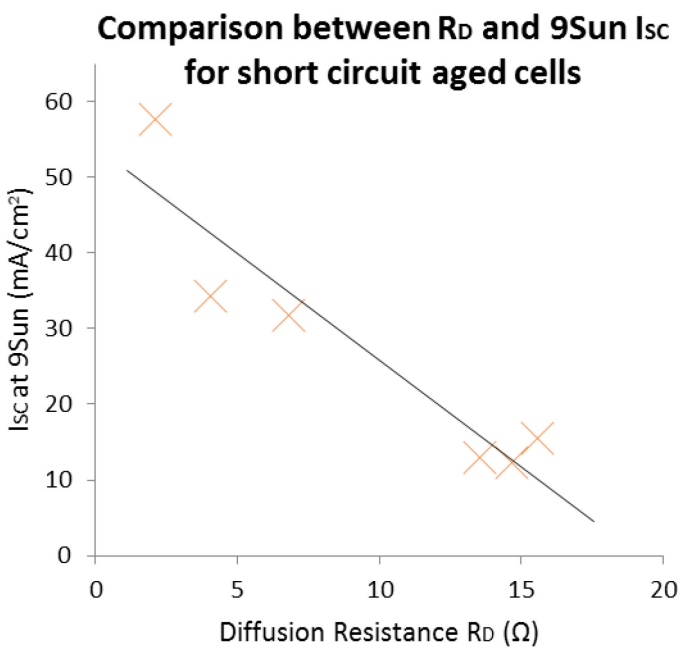

Figure 22 The short circuit current as a function of the diffusion resistance for the aged short circuit cells. The short circuit current values were taken from the 9 Sun equivalent illumination. The black line is the trendline fitted to the data points. All of the short circuit cells are not included in this analysis because the diffusion resistance could not be measured accurately for all of them.

The decrease in charge carrier concentration was studied further with image analysis. The evolution of average blue values of the analyzed electrolyte area is displayed in Figure 23. The data is given relative to the initial case to simplify the studying of the graph by eliminating any initial differences between cell groups. The blue pixel values increased in all of the cell groups aged in different circuit states. The actual rate of increase, i.e. the rate of electrolyte bleaching, was dependent on the state the cells were aged in. Right from the beginning, after four days of aging, the cells aged in short circuit clearly bleached faster than the other groups. This difference remained through the whole 1000 h aging since the short circuit cells had clearly higher blue-value than the others did. The cells under load and in an open circuit bleached slower and their bleaching progress was similar to each other. Only towards the end they began to separate so that the cells under load were slightly more bleached. The rate of bleaching was almost linear in all of the cell groups, except for the short circuit cells. In their case the bleaching slowed down after the first two measurements, but still remained faster than for the other cells.

The last measurement at 1080 h displays strange behavior: it appears that the bleaching has been reversed in all of the cells. According to that data, the color of the electrolyte has darkened back to the level it was after two weeks of aging, which is not very probable. No such changes to the aging system, the measurement methods or the order of measurements were introduced between the last two measurements, which could account for any regeneration of the cells. More likely explanation to this change in the blue value is a measurement error. Since the values are systematically lower for all of the cells, it is probable that the

error was caused by dimmer lighting conditions during the last measurement. Four LED lamps handle lighting during the image analysis photographing and it is possible that one or more of these lamps was accidentally set to lower illumination intensity than was intended. Other possibility is that the remaining charge in the rechargeable batteries powering the lamps was low, leading to lower light intensity. These types of errors in light intensity usually become apparent only after the analysis since human eye is not sensitive enough to detect them during the measurement.

Disregarding the blue values of the last measurement at 1080 h, the image analysis results support the data presented above. All of the cells, but especially those aged in short circuit, were bleached during the aging. Bleaching is contributed to the loss of tri-iodide I_3^- [39], and the results discussed previously in this chapter support the loss of tri-iodide redox mediators as the reason for faster degradation in DSCs aged in short circuit when compared to aging in open circuit or under load.

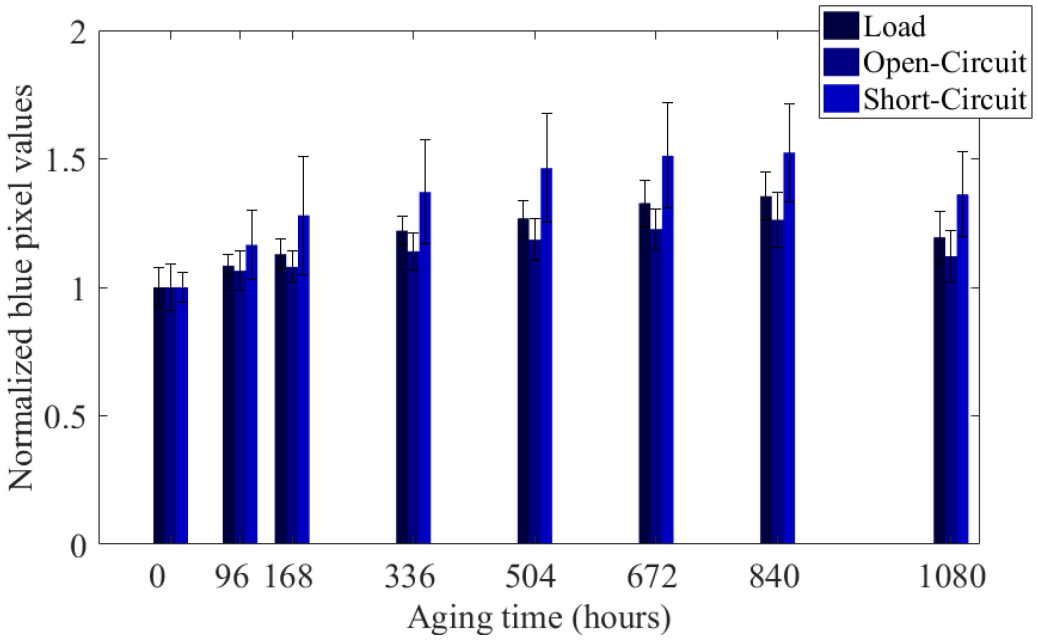

Figure 23 The B-values (blue) of the RGB of the electrolyte during the aging. The B-values are normalized with respect to the initial situation. The height of the bar gives the average from all of the cells in a group and the error bars display the standard deviation between individual cells.

The RGB values presented above were taken from a small area of the electrolyte, but similar analysis was performed also on the whole area of the photoelectrode (see Figure 8). The goal was to discover any possible gradients in the bleaching of the electrolyte. An earlier hypothesis suggested that, in the short circuited cells, the charge carriers diffuse from the edges of the cells to the photoelectrode. Thus, the photoelectrode would be relatively darker in those cells compared to the other cases. However, this was not the case and the B values calculated from the photoelectrodes displayed similar trends as in the Figure 23 above. The electrolyte at the photoelectrode was also bleached most in the cells aged at the short circuit and the bleaching for load and open circuit cells was similar. Due to the similarity with the figure above, the data on bleaching of the electrolyte at the photoelectrode is not presented here.

The bleaching of the electrolyte could be further confirmed by measuring the transmission of light through the electrolyte of the cells. The transmission

through each of the cells between 320 nm and 500 nm wavelength is presented Figure 24. Initially none of the cells allow any light with shorter than 400 nm wavelength through. On longer wavelengths, the transmitted share increases linearly to about 60% at 500 nm. After the aging larger amount of light is transmitted through the cells: all of the cells have a small transmission peak in the UV region, and the rate of increase is no longer linear after 400 nm. The transmission increases quickly after 400 nm until about 450 nm, after which the increase of transmission slows down and is again roughly 60% at 500 nm. The aging increased also the variation in the transmission spectra of the cells, thus in some of the cells the transmission was lower than in the initial case. This can be caused by for example accumulation of dirt on the cell surface. The transmission was especially increased in some of the cells aged in open circuit. In these cases, a significant amount of light was transmitted even below 400 nm wavelength. This agrees with the results from the image analysis, which were discussed above.

There is visible oscillation at higher wavelengths in the individual transmission spectra of Figure 24. This could be caused by the glass substrates of the cells acting as Fabry-Pérot interferometers, with transmitted and reflected light beams of the measurement device interfering constructively (local maxima) and destructively (local minima) [42].

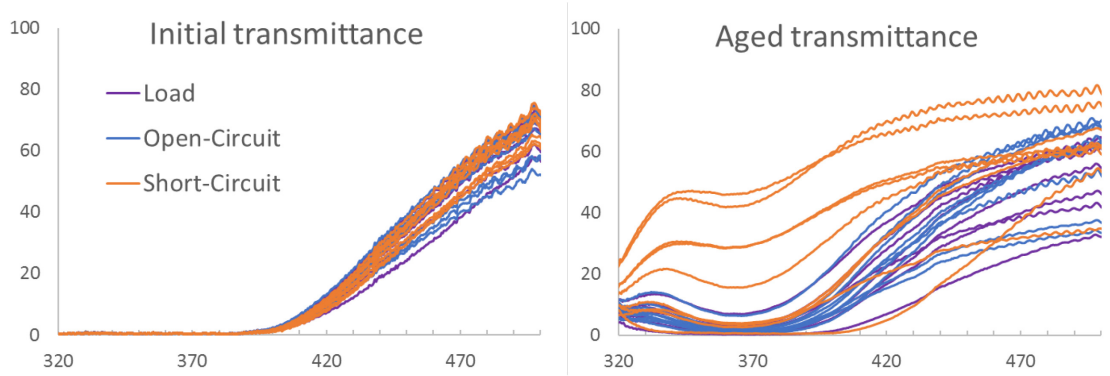

Figure 24 The initial and final transmittances through the electrolytes of the cells aged in different circuit conditions. The displayed wavelength range was chosen from 320 nm to 500 nm since that is the region where the most interesting changes occurred. The oscillations in the data at the higher wavelengths is likely caused by optical phenomena in the glass.

Here we shortly gather and discuss the results of aging DSCs with different external circuits under 1Sun illumination without UV light. While all of the cells were clearly affected by the 1000 hours of light soaking, the cells placed in short circuit were damaged most by the aging, whereas the degradation processes of cells in open circuit and under load were very similar: the efficiency of cells aged in open circuit and under load decreased from 5.0% to 4.2% and the cells in short circuit decreased from 5.0% to 3.2%. Further measurement and analysis of the cells revealed the reason for the degradation to be the loss of tri-iodide I_3^- redox mediators. As the concentration of the redox mediators decreased, transporting charge across the electrolyte became more and more limited which became apparent as an increase of diffusion resistance and the appearance of the limiting current at higher illumination intensities.

Then what was the exact cause of faster degradation of charge carriers in the short circuited cells? This was discussed extensively by S. Mastroianni et al. in their paper on comparison of indoor and outdoor stability testing for DSCs [43]. Their comparison was between cells aged in open circuit and under maximum power point load but the situation can be applied here, only the difference between the cell groups is stronger with cells in short circuit than under load. The

most obvious difference between cells aged in open circuit and the others is that the circuit is not complete. As the electrons, which are excited in the dye and injected to the TiO_2, cannot be collected into the external circuit, they have to eventually recombine with the oxidized charge carriers of the electrolyte (I^-). This kind of operation does not generate external current and involves only the photoelectrode and the electrolyte of the DSC. In the other cases, especially with short circuit aging, the circuit is complete and the whole cell is involved in the current generation process as described in chapter 2.1. This complete operation generates a concentration gradient of charge carriers in the electrolyte, so that there is a higher concentration of I_3^- close to the photoelectrode and lower concentration of them close to the counter electrode [44]. It is suggested that the higher concentration of I_3^- at the photoelectrode favours reactions between them and thiocyanate ligands (SCN^-) in the dye and accumulation of I_3^- in the TiO_2 layer. Both of these reactions would cause decrease in the overall amount of charge carriers, which would lead to the bleaching of the electrolyte and decrease of the cell performance [43]. Higher currents through the cell would lead to a higher I_3^- gradient, which in turn would cause the abovementioned degradation mechanisms to occur at a higher rate, bleaching the electrolyte faster. This is why the bleaching and degradation is fastest in the cells aged at short circuit, where the current is at its maximum. Note that bleaching is present also in the cells aged at open circuit, so the degradation processes caused by the gradient of charge carriers are not the only causes for bleaching; they only increase the rate at which it occurs. Reactions such as the formation iodate [21] would occur regardless of any concentration gradients [43].

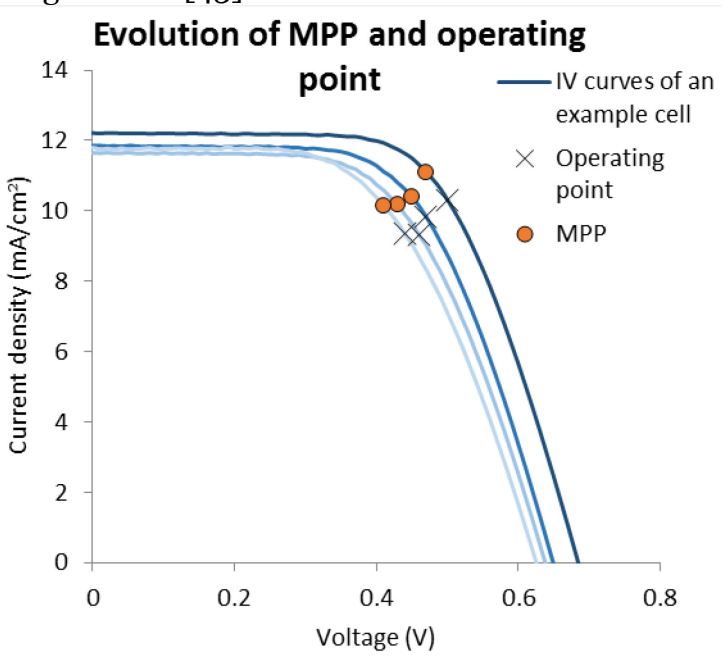

Figure 25 The IV curves from four measurements of an example cell aged under load. The MPP in each case is displayed with orange dots and the operating point to which the cell was set to by the 120 Ω resistor with crosses. The measurements shown here are from 0h, 336h, 672h and 1080h.

There are several other aging studies where the circuit state of DSCs in aging is varied. In the study mentioned above [43], the cells were aged in open circuit and at maximum power point (MPP). The MPP load was created with static resistors as in this study. Comparing the results of [43] and this study, we see a clear difference between the obtained results. Here, there was practically no

difference between the aging of cells in open circuit and under load. In [43] however, the cells in MPP degraded clearly faster than the cells in open circuit. The rate was comparable to the short circuit cells of this study. More differing results were reported in another study: according to [23], where cells were aged in open and short circuits, the cells in short circuit survived an aging of 180 days under illumination better than the cells in open circuit. That is a strange result since no other study reports similar findings and the results are contradictory to the suggested theory of accelerated aging by completed circuit presented above. The components of the DSCs used in that study were slightly different and the cells were assembled in a different, so called monolithic structure. These differences could cause differing aging phenomena. A third article [19] reports results similar to the ones obtained in this study: cells aged in outdoor conditions performed similarly when they were aged in open circuit or at MPP. If the cells were short circuited however, they degraded clearly faster compared to the other cases.

Overall, according to results obtained here and in most of the other studies, it seems clear that commonly DSCs under constant illumination degrade fast in short circuit condition and are relatively stable when aged in open circuit. When the cells are aged close to their MPP with the help of resistors, the results diverge. In some of the studies, cells aged in MPP behaved like the cells in open circuit, while in others they degrade much faster and imitate the behaviour of cells aged in short circuit. The DSCs used in the different studies had small differences in the cell components, such as different dye, which could be the cause for faster bleaching of the electrolyte and degradation of cell performance. Other possible reason is the method how the MPP circuit state was formed. In this and the other studies the maximum power point load was formed simply by adding a resistor, with resistance close to the value required by MPP calculated as in equation *(9)*, to the circuit with the DSC. It is unlikely that in this case the cells were accurately at the MPP. For example, the largest initial difference between the MPP and the attached resistor in this study was 10 Ω. The difference between the operating point and the actual MPP during the aging for an example cell is shown in Figure 25. From the figure, it is clear that even a small difference in the load can shift the operating point away from the MPP. The aging did not have a large effect on the relative locations of the two points since it decreased both the current and voltage of the MPP. It seems that it is important to choose the resistance accurately when attempting to reach the MPP; otherwise the cell may end up surprisingly far from the actual MPP. The differences between the studies may be caused by following situation: in the studies where the cells in MPP performed similarly to the open circuit case, like in this study, the resistors set between the electrodes had too high resistance, causing a higher voltage and thus less current to flow through the cell. Then the operation of the cell would be closer to the operation in open circuit condition, which would lead to a similar aging process. In the opposite case the resistors have too low resistance, leading to a higher current and to operation closer to the short circuit cell and thus to faster degradation. Somewhat curiously the operating current in the loaded cells was still as much as 75…80% of their short circuit currents. Therefore, if the accelerated aging is caused by higher current, the effect at least cannot be linear. Otherwise, the cells under load would have performed much worse. These hypotheses would have to be confirmed experimentally, for example by aging cells in circuit with resistors slightly above and below the resistance values corresponding to the MPP. In the other aging studies of this work, the cells are aged in open circuit to avoid the aging

mechanisms associated with complete circuits. This allows the study to focus on the effects of the different added materials on the cell performance.

4.2. Polymer impurity absorbers

The effect of PMMA on DSC operation was tested in a separate initial experiment, which included only IV measurements during a UV aging. In PMMA cells the PMMA polymer was dissolved into the electrolyte. The results are shown below in Figure 26. The IV behavior of the cells with PMMA in the electrolyte was very similar to the behavior of reference cells. Initially, the short circuit current increased for both cell types, increasing the efficiency. This phenomenon is typical to DSCs and is linked to the generation of surface states on the TiO_2 [45]. After the initial increase, the current quickly decreased at around 200 h by half of its maximum value. The open circuit voltage initially decreased in both cell types and stabilized after about 200 h. Fill factor followed similar trend, decreasing from 0.70 to 0.55 during the first 200 hours and then stabilizing there for the rest of the aging. The efficiency followed closely the development of the short circuit current, increasing initially to almost 4% and decreasing quickly afterwards to below 2%. Overall, this demonstrates a common behavior for DSCs under UV aging: initial increase of performance as the surface states are generated, followed by quick decrease when the charge carriers of the electrolyte degrade [7]. In the end, electrolyte with added PMMA-polymer performed as was hypothesized: this relatively inert polymer caused no adverse effects to the operation of the cell but neither did it improve its long-term stability, nor cause gelling of the electrolyte, which would improve mechanical stability. Thus it was decided that PMMA would not be used in further trials. It should be noted that in another study [46] contradictory results were obtained: a polymer blend electrolyte of 10% PEO and 90% PMMA greatly increased the stability of DSCs. However, the article did not mention how the cells were aged i.e. whether they were illuminated and did the illumination include UV light. The difference in stability in the article could also be caused by leaking of the liquid electrolyte.

The rest of the absorber polymer cells were measured in a separate test series, which was likewise aged in UV light. The IV results for this group are displayed in Figure 27. From the IV results, it is clear that the cells with impurity absorbers performed poorly compared to the reference cells. Even though their short circuit current and open circuit voltage are initially comparable to the references, the fill factor of all of the absorber polymer cells are more than 0.1 lower, which results in about 1%-point decrease in efficiency. The differences become clearer as the cells are aged in the UV light. While the open circuit voltages remain relatively constant during the aging, the short circuit currents decrease to half of their original value. The change is most rapid between 100 and 200 hours, which is reflected into a more rapid decrease of efficiency during that time period. Of the polymer electrolytes, the drop-cast PAA (DC-PAA) seems to fare best. Its open circuit voltage and initial short circuit current are equal to the reference cells and only the lower fill factor causes worse efficiency. The DC-PAA series remains the best polymer absorber throughout the whole aging. It is still clear that the addition of all of the absorbers had a negative impact on the performance of the cells. The causes of this lowered performance are studied further with IPCE and EIS measurements.

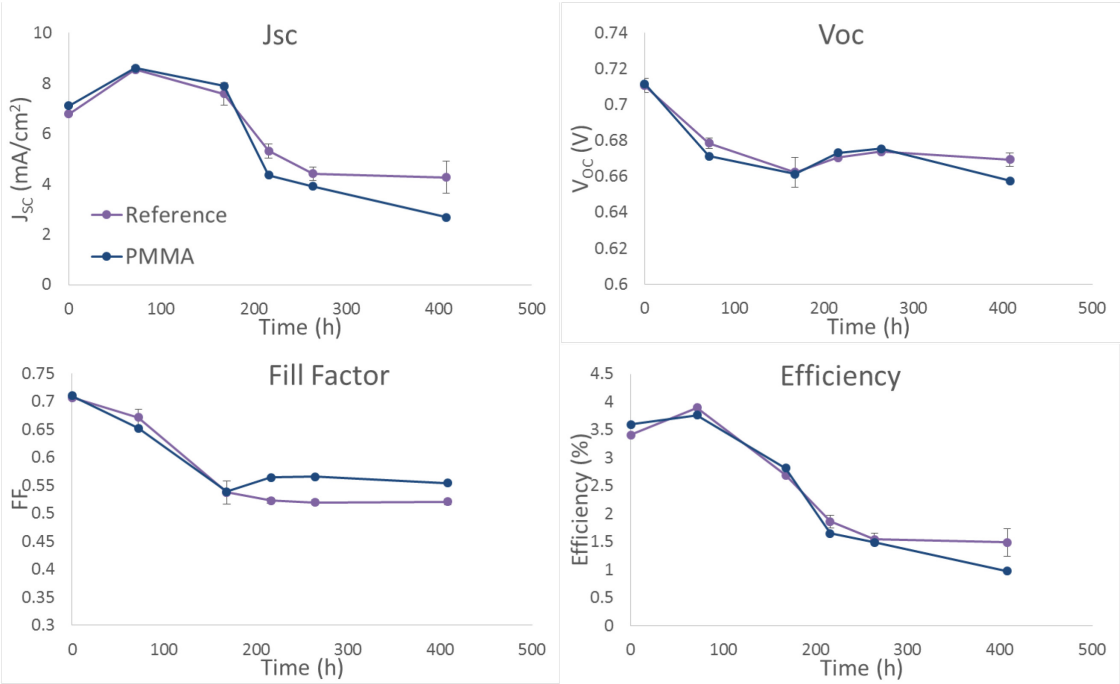

Figure 26 The cell parameters of reference cells and PMMA cells during UV aging.

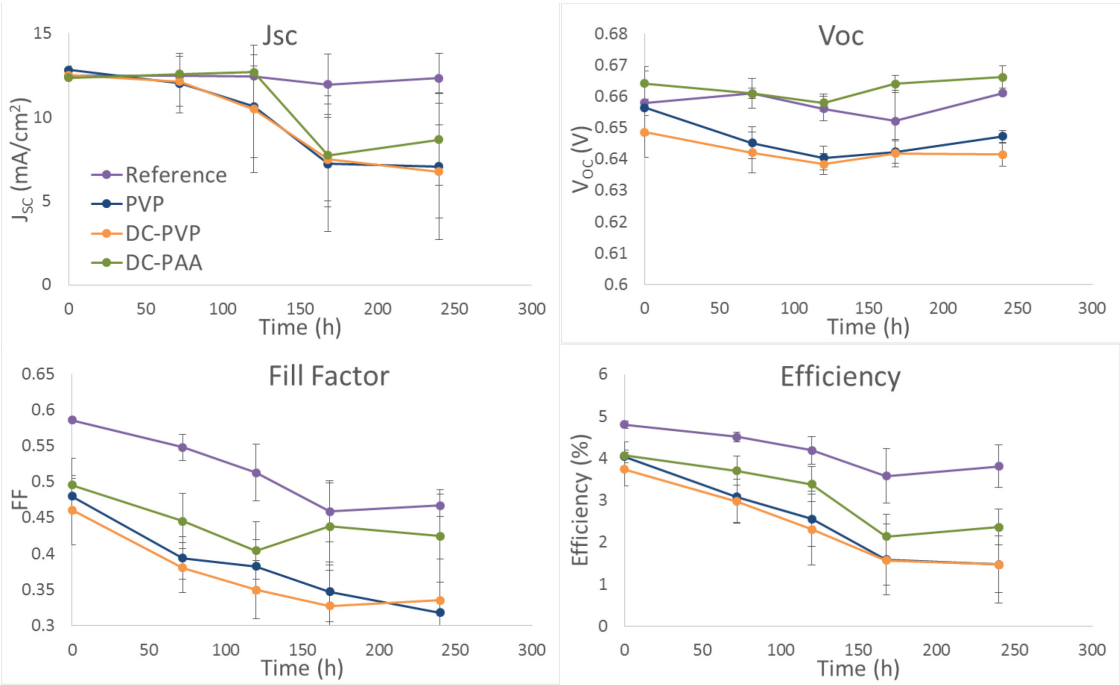

Figure 27 The IV parameters of reference, PAA and PVP cells. 'DC' in front of a polymers means that the polymer was drop-cast on the counter electrode of the DSC instead of being dissolved into the electrolyte.

To study whether the absorber polymers have any effect on the current generation capabilities of the DSCs, The IPCE of the cells in the aging test was measured before and after the UV aging. The IPCE spectra are presented in Figure 28. From the initial curves, we can see that all of the cells in all of the groups had similar IPCE response, aside from one slight outlier in the DC-PAA group. The IPCE remained similar through the whole aging, and at the end of it, the cells still gave a similar IPCE response. The aging did affect the shape of the IPCE curves: After the aging IPCE was increased in all of the cells around wavelength of 400 nm, otherwise the shape and magnitude remained roughly the

same. The increase of IPCE at 400 nm is a common phenomenon in aged iodine based DSCs, and is caused by the bleaching of the electrolyte. As the yellow color of the electrolyte disappears, more the transmittance of the electrolyte improves in the 400 nm region. This increases the amount of light that reaches and is absorbed by the dye, thus improving the IPCE in that region [47] [48]. Overall, the polymer absorbers did not affect the performance of the photoelectrode, so the decrease in efficiency has to be caused in another part of the cell.

In addition, the impedance spectra of the absorber polymer cells were measured initially and after the aging. Three of the parameters calculated from the Nyquist curves are plotted in Figure 29. Unfortunately, the EIS spectrum was so garbled in many of the polymer cells after the aging that the resistance values could be extracted only from few of the cells. The changes in the ohmic series resistance (Rs) are minimal for all of the cell groups. In fact, it appears that the aging decreased the series resistance: initially in all of the cells it was between 25 Ω and 30 Ω, but after the aging it had decreased to 15-20 Ω in the polymer cells. There was surprising amount of variation in the series resistance of reference cells, although in that case the average had decreased slightly as well. The counter electrode-electrolyte interface resistance (R_{CE}) remains stable in the reference cells, staying at around 20 Ω. Instead in the absorber polymer cells, especially in the case of dissolved PVP, R_{CE} was greatly increased. It is not clear what caused such clear difference between dissolved and drop-cast PVP, especially since all the drop-cast PVP should be dissolved to the electrolyte by the end of the aging and thus the electrolytes would be similar. Similarly, the diffusion resistance R_D demonstrated a manifold increase in all of the polymer cells while in the reference cells it merely doubled during the aging. From these results, it becomes apparent that the accelerated decrease in cell performance was caused by detrimental reactions in the electrolyte and at the counter electrode-electrolyte interface.

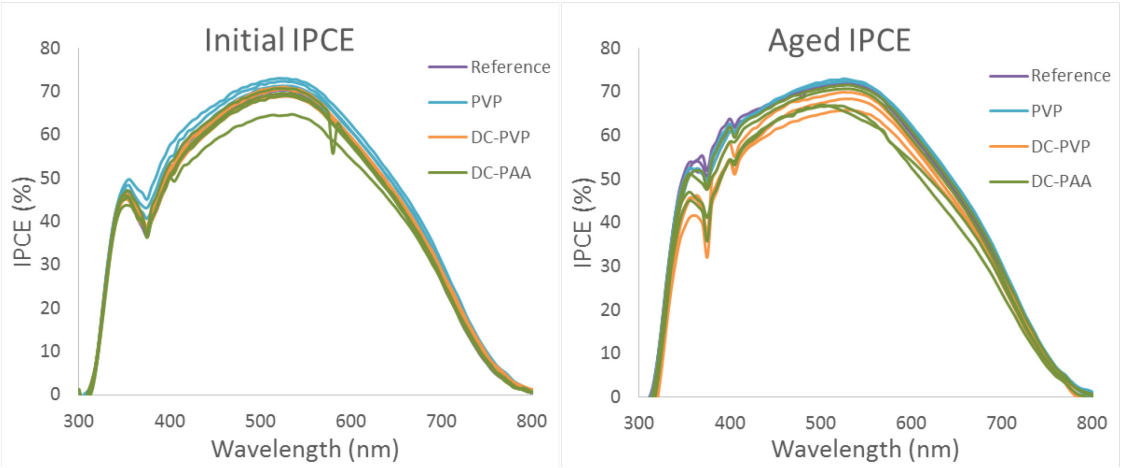

Figure 28 The IPCE spectra of the cells with impurity absorber polymer cells before and after the UV aging. The small oscillations in the data are likely caused by flickering of the IPCE device light source.

In the end, the polymer absorbers did not perform as was hypothesized: instead of increasing cell stability by acting as an internal cleaning agent, the absorber polymers decreased the cell performance and increased the rate of cell degradation. This effect is likely caused by some reaction between them and the electrolyte, which will not be studied further in this work. With these results, it has to be stated that PVP and PAA are not suitable additions to DSCs as such.

However, both PVP and PAA have been used in other DSC studies. PAA was used with poly(ethylene glycol) (PEG) to form a hybrid polymer thermosetting

gel. This gel was used to absorb iodine electrolyte and then it was placed within the cell during assembly. This method resulted in slightly lowered current and efficiency but significantly improved stability [49]. It shows that PAA can be used in a useful manner to improve DSCs. PVP was used for a similar purpose in [50] as in this study. The goal in [50] was to create a gel electrolyte, which also had self-cleaning qualities. As in this study, the outcome in the article was not favorable to PVP: it turned out that the addition of enough PVP to create a gel electrolyte causes substantial decrease in cell performance. One possible reason for the failure of PVP in iodine DSC electrolyte is the formation of a complex called povidone-iodine [50]. Povidone-iodine is an efficient disinfectant used in medicine, but in DSCs it is likely that when iodine reacts with an additive within the electrolyte, charge transport through the electrolyte suffers.

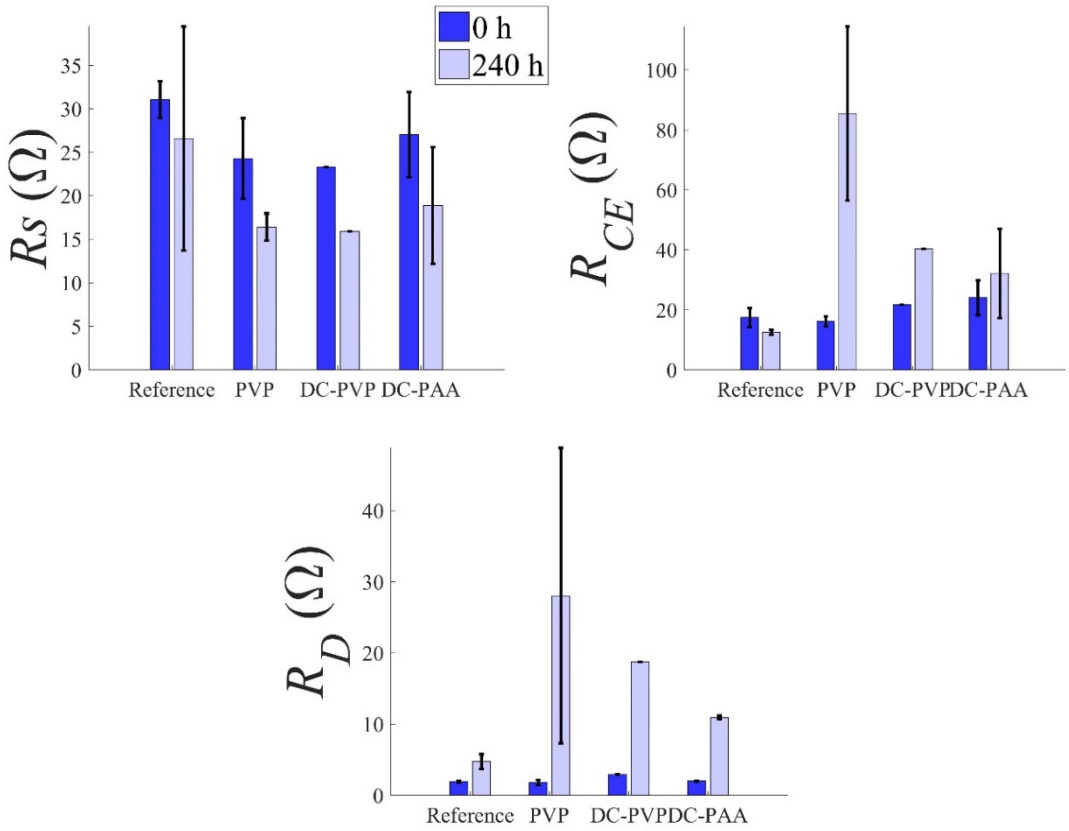

Figure 29 Internal resistances of the impurity absorber polymer cells before and after UV aging. 'DC' in front of the name of the cell group indicates cells for which the polymer was drop-cast instead of being dissolved into the electrolyte.

4.3. Biomaterial aerogels

Like the polymer absorber cells, the cells with biomaterial membranes were aged under UV light. When the biomaterial cells had been aged under UV light for 216 hours, the efficiency of all of the cells had degraded to about 1% or less. The aging study was ended at that point. The IV curves of one typical example cell from each of the groups are shown in Figure 30, both in initial condition and after the aging. The numerical values of cell parameters are calculated and collected as averages and their standard deviations into Table 2. The aging is further visualized by plotting the cell parameters as a function of time in Figure 31. Figure 30 also

includes the initial IV curve of the one cell that was built with TEMPO-aerogel. Only one such cell was assembled because initial trials had given reason to suspect it would not function. This turned out to be indeed the case as can be witnessed by the low current and poor fill factor of its IV curve. When the TEMPO membrane came in contact with the electrolyte, small black areas immediately appeared on its surface. These can still be seen in Figure 32. This would suggest that the electrolyte reacted with something in the TEMPO membrane, possibly with some leftover chemicals from the TEMPO oxidation. Further analysis of TEMPO cells was ended with these results.

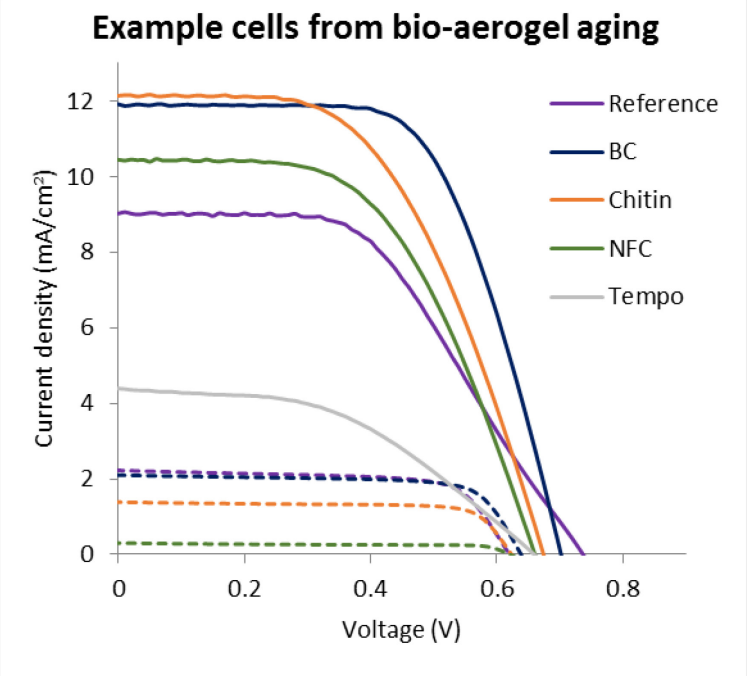

Figure 30 Initial and final IV curves of example cells from each of the cell groups. Solid lines are from the initial measurements and the dashed lines are from after the aging. Small oscillation in the current of initial data is likely caused by slight flickering of the measurement lamp.

Table 2 List of average parameters for each of the cell groups in the aerogel aging test. Both the initial and final values are listed. Also shown are the standard deviation of each of the averages.

Cell group	State	I_{SC} [mA/cm^2]	V_{OC} [mV]	*FF* [%]	Eff [%]	R_{cell} [Ω]
Reference	initial	9.2 ± 0.2	736 ± 7	50 ± 0.3	3.4 ± 0.05	86.0 ± 4.7
	216 h	2.3 ± 0.5	624 ± 3	69 ± 1	1.0 ± 0.2	102 ± 15
BC	initial	11.6 ± 0.2	698 ± 5	60 ± 2	4.9 ± 0.2	41.3 ± 4.0
	216 h	1.7 ± 0.4	633 ± 3	73 ± 1	0.8 ± 0.2	98 ± 19
Chitin	initial	12.0 ± 0.1	680 ± 3	53 ± 1	4.3 ± 0.1	46.5 ± 2.4
	216 h	1.1 ± 0.3	628 ± 4	76 ± 1	0.5 ± 0.1	129 ± 38
NFC	initial	10.5 ± 0.1	662 ± 3	51 ± 4	3.6 ± 0.3	55.7 ± 11
	216 h	0.5 ± 0.1	623 ± 3	78 ± 2	0.2 ± 0.1	213 ± 58

It is also notable that initially the performance of the reference cells was lower than in any of the other biomaterial cells. While the short circuit current *Isc* was around 12 mA/cm² in the BC and Chitin cells, in the reference cells it was only around 9.2 mA/cm² on average. This is not caused by the aerogels themselves, but rather by the method of electrolyte filling used for the different

cells. In the case of liquid reference cells, the electrolyte is injected into the space between the two electrodes. As the cell is filled, the liquid electrolyte is filtered by the nanoporous TiO_2 layer. This causes accumulation of electrolyte additives to the surface of the photoelectrode, resulting in differing performance [51]. It has been shown that especially the accumulation of the voltage-increasing agent (in this case NMBI) on the photoelectrode causes decrease in the current of the cell by restricting electron injection [13]. This is likely the case here as well, since by looking at Figure 31 we see that while the current of the reference cells is initially low, their open circuit voltage is higher than in the other cell groups. In the biomaterial cells, the electrolyte was inserted into the cell by directly dropping it on the aerogel on top of the photoelectrode and then sealing the cell. This method will not cause any electrolyte flow in the cell and thus there is no significant filtering effect. Without filtering, the components of the electrolyte are spread equally to all parts of the cell and this results in a higher initial efficiency [13]. As the cells were aged the reference cells caught up to, and eventually surpassed, the performance of the aerogel cells. This is most likely due to desorption of the filtered additives from the surface of the photoelectrode. During the aging, the bacterial cellulose (BC) cells also improved slightly initially, and then followed closely the aging process of the reference cells. In fact, all of the IV parameters of BC cells were very close to the reference cells, which is very promising for the viability of BC as a DSC electrolyte membrane.

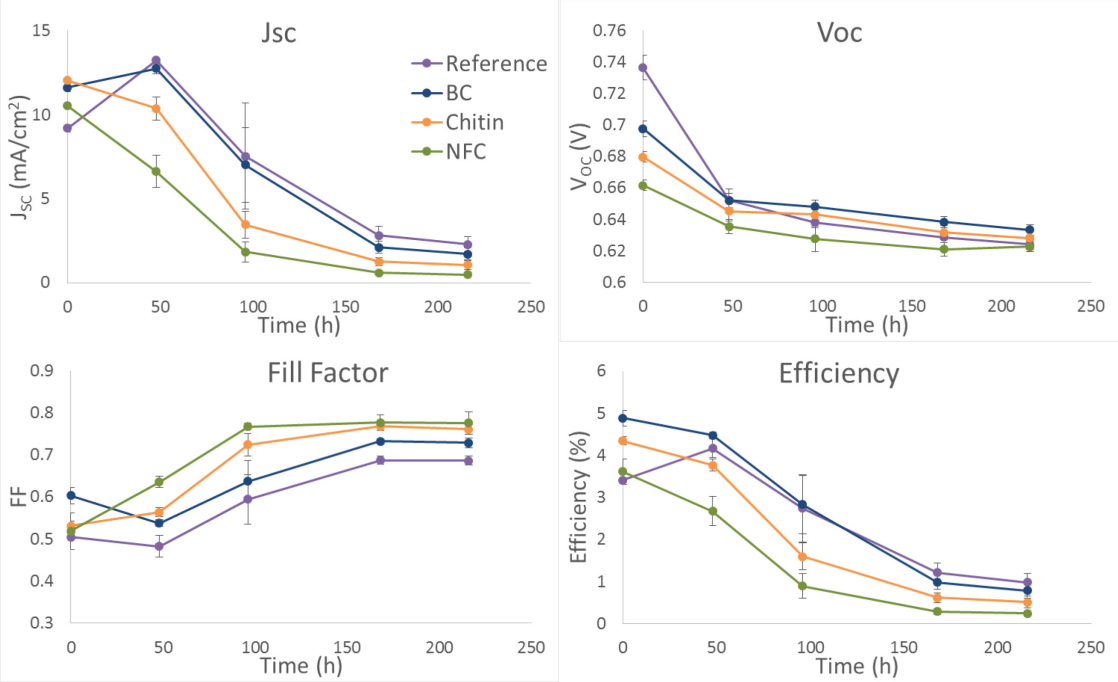

Figure 31 Average cell parameters as a function of time for each of the cell groups in the aerogel aging test. These measurements were performed three times a week.

The aging of chitin and NFC did not yield as promising results: the short circuit current of both cell types decreased instead of increasing initially. When the short circuit current of BC and reference cells started to decrease, it decreased at similar rate also in the chitin and NFC cells. As chitin and NFC started from lower I_{SC} value, they reached very low currents faster than the other cell types. The open circuit voltage V_{OC} remained relatively stable during the aging in all of the cell groups, decreasing from a range of 0.66 V...0.72 V to 0.64 V between the first two measurements and staying there for the rest of the aging. Fill factor likewise performed similarly in all of the cell groups: it increased for all of the

cells from around 0.5 and stabilized in the range 0.7…0.8. It is possible that the fill factor improves as the current of the cell decreases since some recombination losses are decreased when there is less current flowing through the cell [15]. In this case, the decrease of current is likely caused by loss of charge carriers in the electrolyte, which will be discussed more later in the chapter. Even though the fill factor increased, the loss of current was so substantial by comparison that it dominated the effect on efficiency. As a result, the aging behavior of the cell efficiencies is similar to the behavior of the short circuit currents.

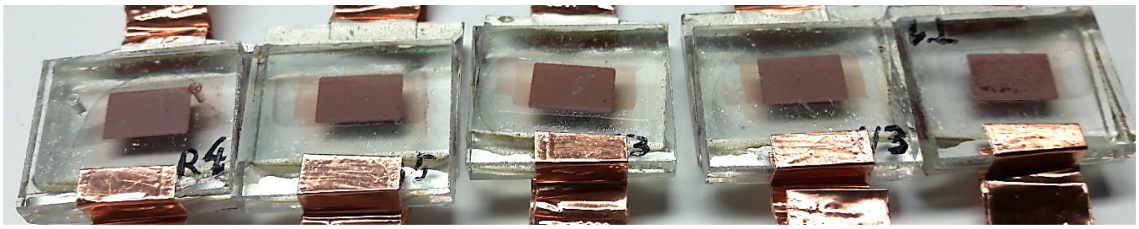

Figure 32 Photograph examples of each of the biomaterial cells after the aging. From left to right: Reference, Bacterial Cellulose, Chitin, NFC and TEMPO. The electrolyte-soaked membrane is clearly visible in BC, Chitin and NFC cells even though the electrolyte is substantially bleached.

EIS was measured thrice during the UV aging of the aerogel DSCs, in the beginning, at the midpoint and at the end. The resulting values of internal resistance components are plotted in Figure 33. Ohmic series resistance *Rs* remained close to the initial value during the aging in all of the cell groups. On fresh cells it was close to 20 Ω, except for reference cells which had a slightly higher value. This difference was probably caused by the filling method of the reference cells as was discussed earlier in the chapter. Eventually the series resistances stabilized between 16 Ω and 19 Ω. Similarly, the aging caused only small changes to the charge transfer resistance R_{CE} between the electrolyte and counter electrode. It steadily increased from between 4 Ω and 6 Ω to between 6 Ω and 8 Ω. While some changes occurred in the R_{CE}, it is not the cause of degradation of the cell performance. Once again, the electrolyte diffusion resistance R_D has increased most obviously during the aging. For all of the cells R_D was initially only in the range of few ohms, but by the end of the aging it had reached about 50 Ω for the reference and BC cells, 70 Ω for the chitin cells and 130 Ω in the case of NFC cells. This is also the order in which the cells performed: reference and BC cells had the highest ending performance and NFC cells the lowest. Thus the reason for the degradation of these cells as well was the decrease of charge transfer capability of the electrolyte.

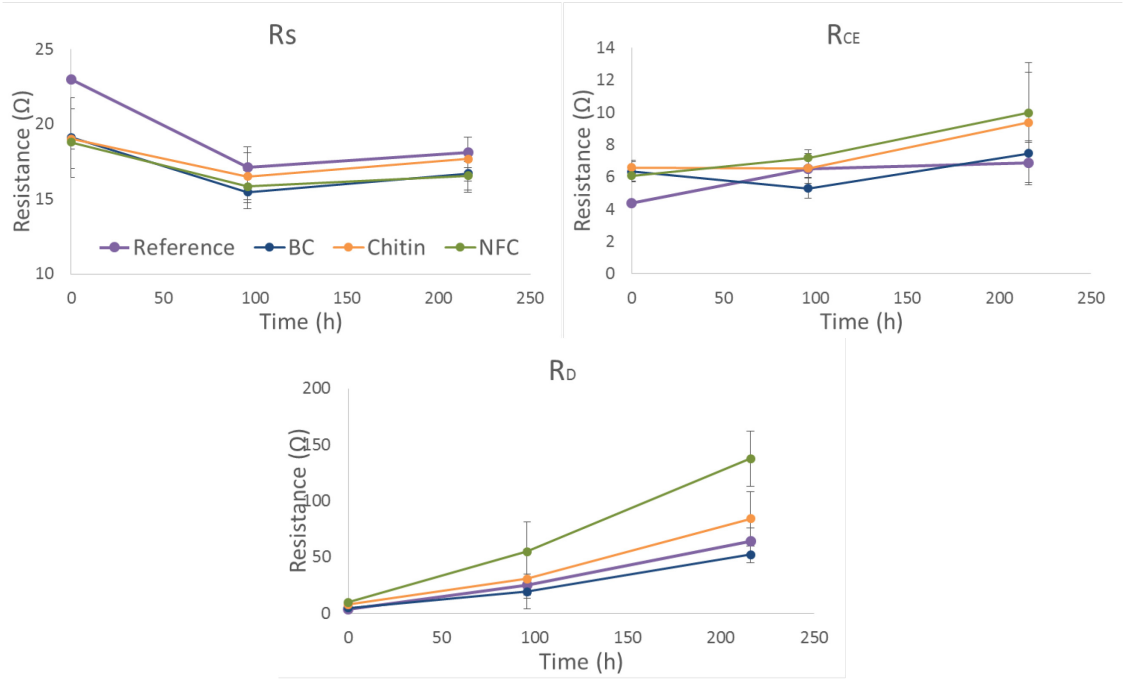

Figure 33 Changes in the internal resistances of the cells with bio-aerogels. As explained before, the values were obtained by fitting a model to the Nyquist curves obtained from EIS measurements.

The initial IPCE curves of all of the aerogel cells are displayed in Figure 34. IPCE data could not be obtained after the aging since the xenon lamp power supply of the IPCE device malfunctioned before the aging test was finished. From the initial spectra we can see clear differences between the cell groups. The shape of the IPCE spectra for all of the cell groups was similar, but the maximum IPCE around 550 nm wavelength was 70% for BC and chitin cells while for NFC and reference cells it was 10 percentage points lower. This makes sense when considering the initial IV results: current that can be drawn from a solar cell is dependent on its IPCE, and the initial short circuit current is higher in BC and chitin cells and lower in NFC and reference cells. In the case of the reference cells this is once again explained by the filling method of the cell. As mentioned before, the injection filling-method causes large amount of voltage increasing electrolyte additives to adsorb on the photoelectrode. These additives increase the voltage of the cell, which simultaneously decreases injection efficiency η_{INJ}, one of the multipliers that form the IPCE of a DSC (equation *(8)*).

Curiously, also the IPCE of NFC cells is decreased compared to the other biomaterial aerogel cells. This is not due to the electrolyte filling method since NFC cells were assembled like the other aerogel cells, which have a higher IPCE. Thus, the most likely explanation is that the NFC creates some detrimental effect that decreases electron injection η_{INJ} or electron collection η_{COL} at the photoelectrode. For example, the contact between NFC and the photoelectrode could attract electrons, leading to electron injection into the NFC instead of the conducting substrate. These electrons would not be utilized in current generation, and that would decrease the IPCE of the cells. Unfortunately, due to the lack of IPCE data from after the aging, we cannot determine if the IPCE behavior of the cells followed the hypotheses presented here. If they did, then the IPCE of the reference cells should have increased to the level of BC and chitin as the electrolyte additives desorbed from the surface of the photoelectrode. As the exact reaction in NFC cells is unknown, it is difficult to predict how IPCE of the NFC cells would have behaved.

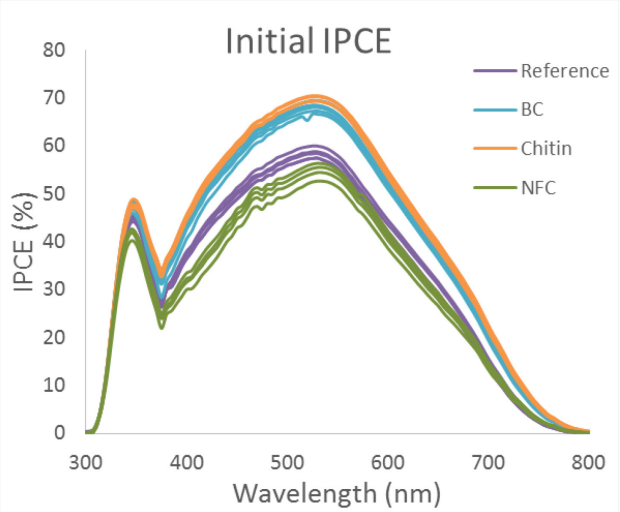

Figure 34 Initial IPCE results of the aerogel DSCs. Small oscillations in the data could be caused by inaccuracies in the calibration of the device or by malfunctioning of the lamp power supply.

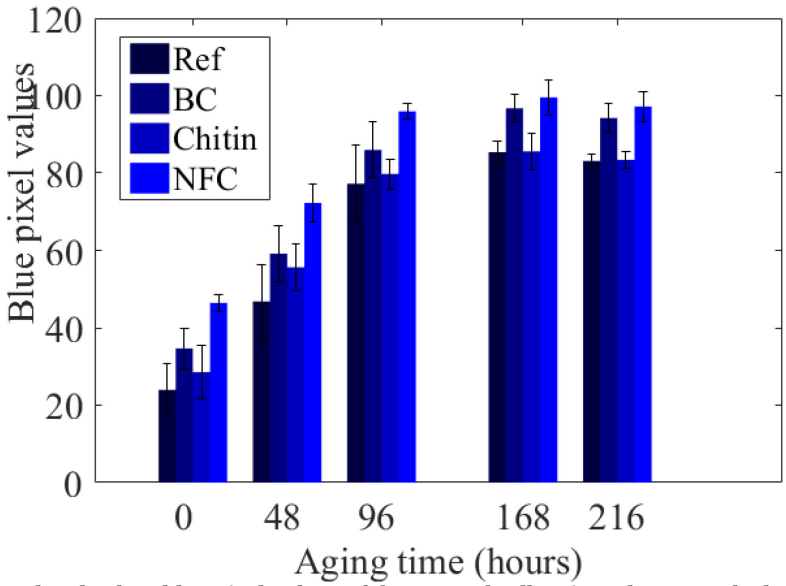

Figure 35 The absolute blue pixel values of the aerogel cells. Since the aerogels themselves affect the coloration of the electrolyte, the values are not fully comparable with the reference cells.

The degradation of the charge carriers was visible as bleaching of the electrolyte in this case as well. This is demonstrated with the blue RGB pixel values in Figure 35. Compared to the circuit state aging, the bleaching in this case was much faster and more severe: the color of the electrolytes had reached their maximum value in only 96 hours, and in the case of the reference cells the magnitude of blue pixel value had more than tripled. This difference is caused by the presence of UV light in the biomaterial aging, which accelerates the cell degradation substantially. The charge carriers continued to still degrade after the values had stabilized, but the imaging technique is not capable of detecting color differences at so low concentrations of iodine [29]. In this case, the cells of the different groups (i.e. reference, BC, chitin and NFC) are not fully comparable against each other since the aerogels themselves alter the color of the electrolyte that they have absorbed. This can be visually confirmed from Figure 32. Because the initial blue values are not comparable across the cell groups, we use the absolute blue pixel values instead of the relative ones.

Despite the different kinds of electrolytes, the electrolytes bleached at similar rates in all of the cells. The different electrolytes also retained their relative positions: the reference and chitin cells, which initially had the lowest blue values, remained 10 and 20 points below BC and NFC, respectively, throughout the aging. This demonstrates that the UV light had no unexpected visible effects on the aging of the iodine electrolyte in the presence of the aerogel membranes.

To sum up the discussion on the biomaterial aerogels, we state that the goal of finding a biomaterial membrane that could be used to ease DSC assembly by absorbing the liquid electrolyte and holding it still was successful with one of the four tested aerogels. Bacterial cellulose films were able to absorb the electrolyte and could be added into the cell without adverse effects on the cell performance. Chitin and nano-fibrillated cellulose likewise managed to absorb the electrolyte, but decreased the performance of the assembled cell, as discussed earlier in this chapter. Finally, TEMPO-oxidized cellulose reacted immediately with the electrolyte and resulted in significantly decreased current and efficiency for the DSC. Even though chitin and NFC decreased the efficiency and current of the cell with their presence, none of the cells accelerated the aging process as can be witnessed by studying the rate of decrease in short circuit current in Figure 31 or by the rate of electrolyte bleaching in Figure 35. In these figures, the rate of change is clearly the same for all of the cell types. It could be said that the effect on cell performance by the biomaterials is ‘passive’ or ‘inert’, in the sense that they do not cause any detrimental reactions. The differing effects on the cell performance by the different types of cellulose films is likely caused by the unequal levels of purity of the materials. As the bacterial cellulose is grown bottom-up from its building materials, the result is pure cellulose after the bacteria and the solvent is rinsed away. Many unknown impurities can remain in the other cellulose materials, which are prepared from woodpulp, without extensive purification. In addition, the impurities themselves are most likely very different from each other, since bacterial cellulose is grown in laboratory conditions and woodpulp is gathered from trees. Different impurities may have differing effects on the operation of the DSCs.

Biomaterials have been used with DSCs in other studies as well. In our earlier study [13] a nanocellulose aerogel was deposited on the glass substrate, with similarly favorable results as in this study. Cellulose has also been used as a gelator in the electrolyte of a DSC [52], demonstrating that biopolymers are capable of performing similar tasks that synthetic polymers are usually used for. Chitin has also seen several applications in DSCs before: like cellulose, chitin has been used to create a gel electrolyte [53]. The compound that gives the chitin shell of a lobster and a shrimp its red color, chitosan, has also been used as a dye in a DSC [54].

5. Summary

This study focused on three different topics: we studied how different external circuits affect the aging of DSCs. The goal of the second topic was to find a way to improve the stability of DSCs by adding absorber polymers into the electrolyte, where they could absorb harmful impurities such as water, thus improving the stability of the devices. The last topic was to streamline the DSC fabrication procedures by adding biomaterial aerogels into the cells, which could hold the liquid electrolyte in its place.

The aging of DSCs in different external circuits revealed that the rate of DSC degradation is clearly dependent on the circuit they are part of. The most stable configuration was to have the cells at open circuit where, since the circuit was not complete, the only operation occurred at the photoelectrodes of the cells. This prevented the degradation mechanisms associated with charge transport through the electrolyte to increase the rate of degradation [43]. The cells aged under a suitable load to imitate the cell operation at the maximum power point (MPP) behaved similarly to the cells in open circuit. There was only a slight decrease in the open circuit voltage, the effect of which on the overall performance of the cell was negligible. It is likely that the current through the electrolyte was low enough to prevent the formation of a large tri-iodide concentration gradient through the cell, which would cause the aforementioned degradation mechanisms to appear and degrade the cell [43]. Finally, the cells in short circuit displayed a greatly increased rate of degradation: the short circuit current of these cells decreased clearly more rapidly than in the other cells and this lead to a large drop in efficiency. The reason for this lowered performance was identified to be the degradation of the tri-iodate charge carriers in the electrolyte. The charge carrier concentration gradient caused by the high current through the cell was clearly harmful to the stability of the cells. These results show that it is important to consider what circuit state is the most relevant for a DSC aging test, as the obtained results are dependent on it. Especially when interested in the aging performance of devices in actual use, it is important to see how they behave under various loads. This aging study could be further improved by setting the MPP more accurately. Here the cells were simply connected to resistors roughly corresponding to the resistance at MPP, but the MPP could be set more accurately by tracking it dynamically. Such methods are described for example in [55]. In this study, the resistances of the resistors were slightly higher than required for reaching the MPP, and this could have decreased the current through the cells so that their degradation rates were decreased. This could be studied by aging cells under two different loads: some cells with a resistor above the MPP resistance and the rest below it. The exact reactions behind the varying effects of the aging on the different cells could be further studied with methods like Raman spectroscopy or liquid chromatography and mass spectrometry [36].

The improvement of cell stability was attempted with three absorber polymers: PMMA, PVP and PAA. Adding PMMA to the cell did not have notable effect on the stability of the cells, probably since it is relatively inert, capable of absorbing only a small amount water with respect to its volume. On the other hand, PVP and PAA had a clear effect on the cell performance. The cells with those polymers performed poorly compared to the reference case. Their performance was already initially decreased by the addition of the polymers, and the situation

continued to deteriorate as the cells were aged. Initially the problem was only the small fill factor but the aging caused fast decrease of the short circuit current as well. It seems likely that the decreased performance was caused by the polymers absorbing or reacting with some necessary components of the electrolyte. The actual effects of the absorbers could be studied further by simply mixing them to the electrolyte and tracking any changes in the electrolyte composition. Finding a suitable impurity absorber material will most likely be very difficult, since it should be selected so that it binds only with the polar water molecules but leaves the charged redox mediators of the electrolyte alone.

Finally, the DSC assembly process was enhanced by introducing an electrolyte- soaked biomaterial aerogel between the electrodes of the cells. One of the aerogels, TEMPO-modified NFC, reacted immediately with the electrolyte and was not suitable to be used in DSCs. The others, i.e. bacterial cellulose, NFC and chitin successfully absorbed the liquid electrolyte and held it in place. The initial performance of the cells assembled with the aerogels suggested that the uneven distribution of electrolyte components, which plagues cells filled by injecting the electrolyte, was not present in the aerogel cells. This proved that cells with aerogels are a viable method to improve the assembly process of DSCs. The NFC and chitin unfortunately decreased the performance of the cells by notably lowering the short circuit current already before the aging. The cells with bacterial cellulose however performed initially better than the reference cells, and during the UV aging they behaved similarly to the reference cells. This demonstrates that the addition of bacterial cellulose aerogels into DSC is perfectly viable method to improve the fabrication of DSCs. This would be especially useful in large-scale modules, where the injection of the electrolyte becomes a problem [51]. The difference between the performances of different biomaterials was likely their purity. Unlike the others, bacterial cellulose is grown with bottom-up methods, allowing purer samples. The effect of the purity of the aerogels could be studied further, to determine exactly which impurities cause the difference in performance and whether they could be removed from the other types of biomaterial aerogels.

6. References

[1] A. V. Herzog, T. E. Lipman and D. M. Kammen, "Renewable Energy Sources," University of California, Berkeley, USA, 2001.

[2] M. Grätzel, "Dye-sensitized solar cells," *Journal of Photochemistry and Photobiology C: Photochemistry Reviews,* vol. 4, no. 2, pp. 145-153, 2003.

[3] R. D. McConnell, "Assessment of the dye-sensitized solar cell," *Renewable & Sustainable Energy Reviews,* vol. 6, no. 3, pp. 273-295, 2002.

[4] B. O'Regan and M. Grätzel, "A low-cost, high-efficiency solar cell based on dye-sensitized colloidal TiO2 films," *Nature,* vol. 353, no. 6346, pp. 737-740, 1991.

[5] S. Mathew, A. Yella, P. Gao, R. Humphry-Baker, B. F. E. Curchod, N. Ashari-Astani, I. Tavernelli, U. Rothlisberger, M. K. Nazeeruddin and M. Grätzel, "Dye-sensitized solar cells with 13% efficiency achieved through the molecular engineering of porphyrin sensitizers," *Nature Chemistry,* vol. 6, no. 3, pp. 242-247, 2014.

[6] S. Yoon, S. Tak, J. Kim, Y. Jun, K. Kang and J. Park, "Application of transparent dye-sensitized solar cells to building integrated photovoltaic systems," *Building and Environment,* vol. 46, no. 10, pp. 1899-1904, 2011.

[7] M. I. Asghar, K. Miettunen, J. Halme, P. Vahermaa, M. Toivola, K. Aitola and P. Lund, "Review of stability for advanced dye solar cells," *Energy Environ. Sci.,* vol. 3, no. 4, pp. 418-426, 2010.

[8] K. Miettunen, J. Halme and P. Lund, "Spatial distribution and decrease of dye solar cell performance induced by electrolyte filling," *Electrochemistry Communications,* vol. 11, no. 1, pp. 25-27, 2009.

[9] E. Figgemeier and A. Hagfeldt, "Are dye-sensitized nano-structured solar cells stable? An overview of device testing and component analyses," *International Journal of Photoenergy,* vol. 6, no. 3, pp. 127-140, 2004.

[10] C. Y. Chen, M. Wang, J. Y. Li, N. Pootrakulchote, L. Alibabaei, C. H. Ngoc-Le, J. D. Decoppet, J. H. Tsai, C. Grätzel, C. G. Wu, S. M. Zakeeruddin and M. Grätzel, "Highly efficient light-harvesting ruthenium sensitizer for thin-film dye-sensitized solar cells," *ACS Nano,* vol. 3, no. 10, pp. 3103-3109, 2009.

[11] P. Wang, S. M. Zakeeruddin, J. E. Moser, M. K. Nazeeruddin, T. Sekiguchi and M. Grätzel, "A stable quasi-solid-state dye-sensitized solar cell with an amphiphilic ruthenium sensitizer and polymer gel electrolyte.," *Nature materials,* vol. 2, no. 6, pp. 402-407, 2003.

[12] M. O. Reese, S. A. Gevorgyan, M. Jorgensen, E. Bundgaard, S. R. Kurtz and e. al., "Consensus stability testing protocols for organic

photovoltaic materials and devices," *Solar Energy Materials and Solar Cells,* vol. 95, no. 5, pp. 1253-1267, 2011.

[13] K. Miettunen, J. Vapaavuori, A. Tiihonen, A. Poskela, P. Lahtinen, J. Halme and P. Lund, "Nanocellulose aerogel membranes for optimal electrolyte filling in dye solar cells," *Nano Energy,* vol. 8, pp. 95-102, 2014.

[14] J. Halme, P. Vahermaa, K. Miettunen and P. Lund, "Device Physics of Dye Solar Cells," *Adv. Mater.,* vol. 22, no. 35, pp. E210-E234, 2010.

[15] K. Hara and H. Arakawa, "Dye-sensitized Solar Cells," in *Handbook of Photovoltaic Science and Engineering (editors Antonio Luque and Steven Hegedus)*, John Wiley & Sons, Ltd, 2003, pp. 663-700.

[16] A. G. Kontos, T. Stergiopoulos, V. Likodimos, D. Milliken, H. Desilvesto, G. Tulloch and P. Falaras, "Long-term thermal stability of liquid dye solar cells," *Journal of Physical Chemistry C,* vol. 117, no. 17, pp. 8636-8646, 2013.

[17] H. Matsui, K. Okada, T. Kitamura and N. Tanabe, "Thermal stability of dye-sensitized solar cells with current collecting grid," *Solar Energy Materials and Solar Cells,* vol. 93, no. 6-7, pp. 1110-1115, 2009.

[18] N. Papageorgiou, W. F. Maier and M. Grätzel, "An Iodine/Triiodide Reduction Electrocatalyst for Aqueous and Organic Media," *J. Electrochem. Soc.,* vol. 144, no. 3, pp. 876-884, 1997.

[19] M. Berginc, U. O. Krašovec and M. Topič, "Outdoor ageing of the dye-sensitized solar cell under different operation regimes," *Solar Energy Materials and Solar Cells,* vol. 120, no. B, pp. 491-499, 2014.

[20] R. Harikisun and H. Desilvestro, "Long-term stability of dye solar cells," *Solar Energy,* vol. 85, no. 6, pp. 1179-1188, 2011.

[21] B. Macht, M. Turrión, A. Barkschat, P. Salvador, K. Ellmer and H. Tributsch, "Patterns of efficiency and degradation in dye sensitization solar cells measured with imaging techniques," *Solar Energy Materials and Solar Cells,* vol. 73, no. 2, pp. 163-173, 2002.

[22] C. H. Kwak, J. H. Baeg, I. M. Yang, K. Giribabu, S. Lee and Y. S. Huh, "Degradation analysis of dye-sensitized solar cell module consisting of 22 unit cells for thermal stability: Raman spectroscopy study," *Solar Energy,* vol. 130, pp. 244-249, 2016.

[23] H. Pettersson and T. Gruszecki, "Long-term stability of low-power dye-sensitised solar cells prepared by industrial methods," *Solar Energy Materials and Solar Cells,* vol. 70, no. 2, pp. 203-212, 2001.

[24] H.-L. Lu, T. F.-R. Shen, S.-T. Huang, Y.-L. Tung and T. C.-K. Yang, "The degradation of dye sensitized solar cell in the presence of water isotopes," *Solar Energy Materials and Solar Cells,* vol. 95, no. 7, pp. 1624-1629, 2011.

[25] K. Zhu, S.-R. Jang and A. J. Frank, "Effects of water intrusion on the charge-carrier dynamics, performance, and stability of dye-

sensitized solar cells," *Energy & Environmental Science,* vol. 5, pp. 9492-9495, 2012.

[26] J. Nelson, The Physics of Solar Cells, Imperial College Press, 2003.

[27] Q. Wang, J.-E. Moser and M. Grätzel, "Electrochemical Impedance Spectroscopic Analysis of Dye-Sensitized Solar Cells," *J. Phys. Chem. B,* vol. 109, pp. 14945-14953, 2005.

[28] M. Grätzel, "Solar energy conversion by dye-sensitized photovoltaic cells," *Inorganic chemistry,* vol. 44, no. 20, pp. 6841-6851, 2005.

[29] M. I. Asghar, K. Miettunen, S. Mastroianni, J. Halme, H. Vahlman and P. Lund, "In situ image processing method to investigate performance and stability of dye solar cells," *Solar Energy,* vol. 86, no. 1, pp. 331-338, 2012.

[30] B. C. O'Regan, J. R. Durrant, P. M. Sommeling and N. J. Bakker, "Influence of the TiCl4 Treatment on Nanocrystalline TiO2 Films in Dye-Sensitized Solar Cells. 2. Charge Density, Band Edge Shifts, and Quantification of Recombination Losses at," *J. Phys. Chem. C,* vol. 111, no. 37, pp. 14001-14010, 2007.

[31] A. Tiihonen, *The effect of electrolyte purification on performance and long-term stability of dye-sensitized solar cells,* Espoo, 2013.

[32] "Matbase," [Online]. Available: https://www.matbase.com/material-categories/natural-and-synthetic-polymers/commodity-polymers/material-properties-of-polymethyl-methacrylate-extruded-acrylic-pmma.html#properties. [Accessed 9 12 2016].

[33] F. Haaf, A. Sanner and F. Straub, "Polymers of N-Vinylpyrrolidone: Synthesis, Characterization and Uses," *Polymer Journal,* no. 17, pp. 143-152, 1985.

[34] "Polyacrylates," Polymer Science Learning Center, [Online]. Available: http://pslc.ws/macrog/acrylate.htm. [Accessed 9 12 2016].

[35] "Products," Sigma Aldrich, [Online]. Available: http://www.sigmaaldrich.com/catalog/. [Accessed 9 12 2016].

[36] A. Tiihonen, K. Miettunen, S. Rendon, D. Mavrynsky, J. Halme, R. Leino and P. Lund, "The Effect of Electrolyte Purification on the Performance and Long-Term Stability of Dye-Sensitized Solar Cells," *Journal of the Electrochemical Society,* vol. 162, no. 9, pp. H661-H670, 2015.

[37] H. A. Khalil, Y. Davoudpour, M. N. Islam, A. Mustapha, K. Sudesh, R. Dungani and M. Jawaid, "Production and modification of nanofibrillated cellulose using various mechanical processes: A review," *Carbohydrate Polymers,* vol. 99, pp. 649-665, 2014.

[38] S. G. Hashmi, M. Ozkan, A. Tiihonen and P. D. Lund, "Very high stability of air-processed inkjet-infiltrated carbon-based printed perovskite solar cells in ultaviolet light soaking," *To be submitted,* 2016.

[39] S. Mastroianni, I. Asghar, K. Miettunen, J. Halme, A. Lanuti, T. M. Brown and P. Lund, "Effect of electrolyte bleaching on the stability and performance of dye solar cells," *Physical Chemistry Chemical Physics,* vol. 16, no. 13, pp. 6092-6100, 2014.

[40] L.-L. Li, Y.-J. Chen, H.-P. Wu, N. S. Wang and E. W.-G. Diau, "Detachment and transfer of ordered TiO2 nanotube arrays for front-illuminated dye-sensitized solar cells," *Energy & Environmental Science,* vol. 4, no. 9, pp. 3420-3425, 2011.

[41] A. Poskela, "Screen Printable Gel Electrolytes for Dye-Sensitized Solar Cells, Special assignment," Aalto University, Espoo, 2016.

[42] H. Tao, Z. Yang and P. Lucas, "Origin of photo-induced transmitting oscillations in chalcogenide glasses," *Optics Express,* vol. 17, no. 20, pp. 18165-18170, 2009.

[43] S. Mastroianni, A. Lanuti, S. Penna, A. Reale, T. M. Brown, A. Di Carlo and F. Decker, "Physical and electrochemical analysis of an indoor-outdoor ageing test of large-area dye solar cell devices," *ChemPhysChem,* vol. 13, no. 12, pp. 2925-2936, 2012.

[44] N. Papageorgiou, P. Liska, A. Kay and M. Grätzel, "Mediator transport in multilayer nanocrystalline photoelectrochemical cell configurations," *Journal of the Electrochemical Society,* vol. 146, no. 3, pp. 898-907, 1999.

[45] B. A. Gregg, "Interfacial processes in the dye-sensitized solar cell," *Coordination Chemistry Reviews,* vol. 248, no. 13-14, pp. 1215-1224, 2004.

[46] E. Aram, M. Ehsani and H. Khonakdar, "Improvement of ionic conductivity and performance of quasi-solid-state dye sensitized solar cell using PEO/PMMA gel electrolyte," *Thermochimica Acta,* vol. 615, pp. 61-67, 2015.

[47] C. Wu, Y. Gong, S. Han, T. Jin, B. Chi, J. Pu and L. Jian, "Electrochemical characterization of a novel iodine-free electrolyte for dye-sensitized solar cell," *Electrochimica Acta,* vol. 71, pp. 33-38, 2012.

[48] J. Wiberg, T. Marinado, D. P. Hagberg, L. Sun, A. Hagfeldt and B. Albinsson, "Effect of anchoring group on electron injection and recombination dynamics in organic dye-sensitized solar cells," *Journal of Physical Chemistry C,* vol. 113, no. 9, pp. 3881-3886, 2009.

[49] J. Wu, Z. Lan, J. Lin, M. Huang, S. Hao, T. Sato and S. Yin, "A novel thermosetting gel electrolyte for stable quasi-solid-state dye-sensitized solar cells," *Advanced Materials,* vol. 19, no. 22, pp. 4006-4011, 2007.

[50] V. K. Singh, B. Bhattacharya, S. Shukla and P. K. Singh, "New Solid-Polymer-Electrolyte Material for Dye-Sensitized Solar Cells," vol. 49, no. 1, pp. 123-127, 2015.

[51] K. Miettunen, I. Asghar, S. Mastroianni, J. Halme, P. R. F. Barnes, E. Rikkinen, B. C. O'Regan and P. Lund, "Effect of molecular filtering and electrolyte composition on the spatial variation in

performance of dye solar cells," *Journal of Electroanalytical Chemistry,* vol. 664, pp. 63-72, 2012.

[52] P. Li, Y. Zhang, W. Fa, Y. Zhang and B. Huang, "Synthesis of a grafted cellulose gel electrolyte in an ionic liquid ([Bmim]I) for dye-sensitized solar cells," *Carbohydrate Polymers,* vol. 86, no. 3, pp. 1216-1220, 2011.

[53] R. Singh, N. A. Jadhav, S. Majumder, B. Bhattacharya and P. K. Singh, "Novel biopolymer gel electrolyte for dye-sensitized solar cell application," *Carbohydrate Polymers,* vol. 91, no. 2, pp. 682-685, 2013.

[54] X. Zhao, G. Xiao, X. Zhang, H. Su and T. Tan, "The Effect of Ni2+ and Cu2+ on the Photocatalytic Degradation of Dyes by the Chitosan–TiO2 Complex," *Appl Biochem Biotechnol,* vol. 168, no. 1, p. 183–197, 2012.

[55] M. Masoum, H. Dehbonei and E. Fuchs, "Theoretical and experimental analyses of photovoltaic systems with voltageand current-based maximum power-point tracking," *IEEE Transactions on Energy Conversion,* vol. 17, no. 4, pp. 514-522, 2002.